

# Fossil and non-fossil source contributions to atmospheric carbonaceous aerosols during extreme spring grassland fires in Eastern Europe

V. Ulevicius<sup>1</sup>, S. Byčenkienė<sup>1</sup>, C. Bozzetti<sup>2</sup>, A. Vlachou<sup>2</sup>, K. Plauškaitė<sup>1</sup>, G. Mordas<sup>1</sup>, V. Dudoitis<sup>1</sup>, G. Abbaszade<sup>3</sup>, V. Remeikis<sup>1</sup>, A. Garbaras<sup>1</sup>, A. Masalaite<sup>1</sup>, J. Blees<sup>2</sup>, R. Fröhlich<sup>2</sup>, K. R. Dällenbach<sup>2</sup>, F. Canonaco<sup>2</sup>, J. G. Slowik<sup>2</sup>, J. Dommen<sup>2</sup>, R. Zimmermann<sup>3,4</sup>, J. Schnelle-Kreis<sup>3</sup>, G. A. Salazar<sup>5</sup>, K. Agrios<sup>5,6</sup>, S. Szidat<sup>5</sup>, I. El Haddad<sup>2</sup> and A. S. H. Prévôt<sup>2</sup>

[1] Department of Environmental Research, SRI Center for Physical Sciences and Technology, Vilnius, Lithuania

[2] Laboratory of Atmospheric Chemistry, Paul Scherrer Institute (PSI), 5232 Villigen, Switzerland

[3] Helmholtz Zentrum München, German Research Center for Environmental Health (GmbH), Joint Mass Spectrometry Centre, Cooperation Group Comprehensive Molecular Analytics and Helmholtz Virtual Institute of Complex Molecular Systems in Environmental Health – Aerosol and Health (HICE), 85764 Neuherberg, Germany

[4] Analytical Chemistry & Joint Mass Spectrometry Centre, Institute of Chemistry, University of Rostock, Dr.-Lorenz-Weg 1, D-18051 Rostock /Germany

[5] Department of Chemistry and Biochemistry & Oeschger Centre for Climate Change Research, University of Bern, 3012 Bern, Switzerland

[6] Laboratory of Radiochemistry and Environmental Chemistry, PSI, 5232 Villigen, Switzerland

Correspondence to: V. Ulevicius and A. S. H. Prévôt ([uleviev@ktl.mii.lt](mailto:uleviev@ktl.mii.lt), [andre.prevot@psi.ch](mailto:andre.prevot@psi.ch))

## Abstract

In early spring the Baltic region is frequently affected by high pollution events due to biomass burning in that area. Here we present a comprehensive study to investigate the impact of biomass/grass burning (BB) on the evolution and composition of aerosol in Preila, Lithuania, during springtime open fires. Non-refractory submicron particulate matter (NR-PM<sub>1</sub>) was measured by an Aerodyne aerosol chemical speciation monitor (ACSM) and a source apportionment with the multilinear engine (ME-2) running the positive matrix factorization (PMF) model was applied to the organic aerosol fraction to investigate the impact of biomass/grass burning. Satellite observations over regions of biomass burning activity supported the results and identification of air mass transport to the area of investigation. Sharp increases in biomass burning tracers, such as levoglucosan up to 683 ng m<sup>-3</sup> and black carbon (BC) up to 17 µg m<sup>-3</sup> were observed during this period. A further separation between fossil and non-fossil primary and secondary contributions was obtained by coupling ACSM PMF results and radiocarbon (<sup>14</sup>C) measurements of the elemental (EC) and organic (OC) carbon fractions. Non-fossil organic carbon (OC<sub>nf</sub>) was the dominant fraction of PM<sub>1</sub>, with the primary (POC<sub>nf</sub>) and secondary (SOC<sub>nf</sub>) fractions contributing 26-44% and 13-23% to the TC, respectively. 5–8 % of the TC had a primary fossil origin (POC<sub>f</sub>), whereas the contribution of fossil secondary organic carbon (SOC<sub>f</sub>) was 4–13 %. Non-fossil EC (EC<sub>nf</sub>) and fossil EC (EC<sub>f</sub>) ranged from 13–24 % and 7–12 %, respectively. Isotope ratio of stable carbon and nitrogen isotopes were used to distinguish aerosol particles associated with solid and liquid fossil fuel burning.

## 1 Introduction

On global scale wood or grass burning is a major source of organic aerosol (Crutzen et al., 1979; Levine, 1996). Approximately 90 % of vegetation burning is caused by human-induced fires (Baldini et al., 2002) and only a minor fraction derives from natural processes such as lightning. The composition of biomass smoke depends on the type of wood, combustion conditions (flaming versus smoldering), and ambient weather conditions (Weimer et al., 2008, Grieshop et al., 2009, Hawkins and Russell, 2010 and Akagi et al., 2012). Fine particles emitted from biomass burning include directly emitted primary particles (POA) and secondary organic aerosols (SOA), formed in the atmosphere as the plume ages through photochemical processes driven by sunlight (Capes et al., 2008, Heringa et al., 2011).

1 Many studies have revealed that organic matter (OM) is the largest fraction of ambient fine  
2 particles, typically comprising 20–90 % of the submicron particulate mass (Jimenez et al.,  
3 2009). Factor analysis of aerosol mass spectra from Aerodyne aerosol mass spectrometer  
4 enables the deconvolution of OM into different factors based on their mass spectral  
5 fingerprints (Lanz et al., 2007; Aiken et al., 2009; Ulbrich et al., 2009;). Such results provided  
6 valuable insights into the source and transformation processes of organic aerosols (OA) in the  
7 atmosphere (Lanz et al., 2010; Ng et al., 2011; Hildebrandt et al., 2011; Canonaco et al. 2013;  
8 Bougiatioti et al., 2014; Huang et al., 2014).

9 The main type of biomass burning in Lithuania and surrounding countries in early spring  
10 during the last years is illegal [grass burning](#) for land clearing (Ulevicius et al., 2010b;  
11 Byčenkienė et al. 2013). The north-east European countries are considered to influence  
12 significantly the microphysical, chemical and optical properties of the aerosol in the Baltic  
13 Sea region (Kikas et al., 2008; Zawadzka et al., 2013; Mann et al., 2014, Beddows et al.,  
14 2014). Long-term measurements of carbonaceous aerosols performed in this area by Ulevicius  
15 et al. (2010a, 2010b) and Byčenkienė et al. (2011, 2013) reported a yearly occurrence of high  
16 biomass burning organic aerosol (BBOA) levels during March–April related to regional  
17 transport from the Kaliningrad region, Ukraine and southwestern part of Russia surrounding  
18 the Black Sea, but information on the nature and chemical composition of the biomass  
19 burning aerosol in Lithuania is still limited. There has been no systematic investigation of the  
20 impact of biomass burning on ambient organic aerosol levels in this region, and a quantitative  
21 estimate is needed to understand the possible impacts of BBOA on air quality in the south-  
22 eastern Baltic Sea region.

23 In many studies levoglucosan was used to assess the contribution of biomass-burning smoke  
24 to the aerosol mass concentrations (Puxbaum et al., 2007). A number of source emission  
25 studies reported that levoglucosan is not a useful tracer after long-range transport due to its  
26 transformation (Hoffmann et al., 2010, Hennigan et al., 2010; Mochida et al., 2010). In  
27 contrast to levoglucosan, determination of radiocarbon ( $^{14}\text{C}$ ) offers a unique possibility for  
28 source apportionment of carbonaceous aerosol particles, as it unambiguously distinguishes  
29 fossil from non-fossil emissions (e.g. Currie, 2000; Ceburnis et al., 2011).

30 For this study, in the framework of the Lithuanian-Swiss Cooperation Programme joint  
31 research project (AEROLIT), an ACSM was deployed in a background area of the South  
32 Baltic Sea to measure airborne submicron particles for one month during a period of frequent  
33 grass burning pollution. The main findings include investigation of OA components (Sects.

3.1–3.2), molecular markers (Sect. 3.2), source apportionment of EC and OC using  $^{14}\text{C}$  data and positive matrix factorization (PMF) of the ACSM organic mass spectra (Sect. 3.3).

## **2 Methods**

### **2.1. Site description and filter sampling**

Continuous air monitoring and time integrated particulate matter sampling were carried out in March 2014 in Preila, Lithuania (55° 55' N, 21° 04' E 5 m a.s.l.) (Fig. 1). Preila is a representative coastal background site, an ideal location for studying the long-range transport of air pollutants in the South-eastern Baltic region due to the absence of significant local sources (Fig. 1, Table 1). It served as a “super site” for the EUSAAR-EU-funded I3 (Integrated Infrastructures Initiatives) project. During the measurement period, strong biomass burning activities were observed on 9–10 March 2014. A high-volume sampler (Digital model Aerosol Sampler DHA-80, 500 l min<sup>-1</sup>) was used to collect PM<sub>1</sub> aerosol particles onto 150 mm diameter Pallflex quartz fibre filters (pre-baked for 24 h at 550 °C) over a 24-hour sampling period. Filters were stored in a freezer (at -20 °C) immediately after sampling.

### **2.2. Instrumentation**

#### **2.2.1 Aerosol Chemical Speciation Monitor and data analysis**

An ACSM (Aerodyne Research, Inc., Billerica, MA, USA) was deployed to measure PM<sub>1</sub> components in Preila (Fig. 1, Sect. 2.1). A PM<sub>10</sub> impactor-type inlet was utilized to remove coarse particles from the sample stream. The sampling air (1.1 L min<sup>-1</sup>) passed through a vertical 2.5 m long stainless steel tube with a 6 mm i.d. and a Nafion dryer (MD-110-12S-4, PermaPure LLC, Toms River, NJ, USA) before reaching the device. Aerosol particle diffusion losses in the sampling line were less than 4.0 % for particles from 40 nm to 1 µm according to Gormley and Kennedy (Baron and Willike, 2001) and the relative humidity lower 50 % (by SATO model SK-L200TH). Thus, the used sampling line and ambient relative humidity did not affect aerosol mass concentration measured by ACSM. The transported aerosol flow was split and directed to a scanning mobility particle sizer (model 19.3.09 IFT/TT (TROPOS, Leipzig, Germany) and to the ACSM. In the ACSM particles were directed onto a resistively heated surface at ~600 °C where NR-PM<sub>1</sub> components are flash vaporized and the resulting gases are subsequently ionized by 70 eV electron impact. ACSM

was operated with a time resolution of  $\sim 28$  min (for typical aerosol loadings, i.e. several  $\mu\text{g m}^{-3}$ ) and a scan rate of  $220 \text{ ms amu}^{-1}$  from  $m/z$  10 to 140 (approximately 31.9 s per scan and 1.126 s pause), 56 scans and data interval 30 min. The data acquisition software used was DAQ 1.4.4.4. The mass concentrations and mass spectra were processed using ACSM standard data analysis software (v 1.5.3.0).

The instrument was calibrated using ammonium sulphate and ammonium nitrate. The determined calibration parameters were response factor (RF)  $\text{RF}_{\text{NO}_3} = 2.75 \times 10^{-11}$  and relative ionization efficiency (RIE)  $\text{RIE}_{\text{NH}_4} = 6.16$ ,  $\text{RIE}_{\text{SO}_4} = 0.92$ . The  $\text{RIE}_{\text{Org}} = 1.4$ ,  $\text{RIE}_{\text{Chl}} = 1.3$  were set as default. However, the ACSM collection efficiency varies depending on the acidity of aerosol particles, aerosol composition, and particle phase water (Matthew et al., 2008). Many atmospheric aerosol studies reported reasonable agreement and linear correlations were obtained with other measurements by using a collection efficiency of 0.5 (Aiken et al. 2009; Timonen et al. 2010). Middlebrook et al., (2012) had proposed a collection efficiency calculation method. The collection efficiency for each measurement and daily mean CE values were calculated. The CE variation was small during the entire measurement campaign (March 2014), so the determined mean CE value was 0.52 with a standard deviation of 0.08, which is very close to other works (Aiken et al. 2009; Timonen et al. 2010). This is not surprising because the sampled aerosol was dried to  $\text{RH} < 50\%$ , moreover, the nitrate fraction was quite low (15% on average) and a high acidity of aerosols was not expected at Preila station (EMEP). Thus, we used the  $\text{CE} = 0.52$  in our investigation. The time series of organic aerosol mass spectra were processed using PMF analysis.

### 2.2.2. PMF analysis

The ACSM measured data were averaged to 1-hour time resolution. A graphical user interface SoFi (Source Finder) (Canonaco et al., 2013), developed at Paul Scherrer Institute was used to perform PMF for the source apportionment of the non-refractory OA mass spectra collected during March 2014. Only signals at  $m/z < 120$  were used for PMF analysis (Paatero and Tapper, 1994; Paatero, 1997)) due to the following reasons: 1) the signals above  $m/z > 120$  account for a minor fraction of total signal, 2) the  $m/z$ 's  $> 120$  have larger uncertainties because of poor ion transmission and the large interferences of naphthalene signals on some  $m/z$ 's (e.g.,  $m/z$  127, 128, and 129) (Sun et al., 2012). A 2-factor solution including a Primary Organic Aerosol factor (POA), and a Secondary Organic Aerosol factor (SOA) was selected for this study. 20 different PMF runs were performed using a bootstrapping approach

(Davison and Hinkley, 1997). The bootstrap creates new input data matrices by randomly resampling measured mass spectra from the original input matrices. Moreover each PMF bootstrap run is initiated from a different pseudorandom starting-point of the algorithm (seed). The bootstrapping approach, together with the seed approach allows a reasonable exploration of the PMF solution space (Paatero et al., 2014). Higher order solutions (3 factors) were explored yielding additional primary profiles, without a significant modification of the secondary contributions. Moreover the retrieved additional profiles showed very high time correlation ( $R^2 = 0.98$ ) with the POA factor, suggesting a splitting of the same aerosol source. As the additional primary factors could not be associated to specific primary emissions, those solutions are not shown. Medium-long range transport of polluted air masses resulted in a co-variability of the sources at the sampling site, hampering a further separation of the primary organic aerosols.

### **2.2.3. 7-wavelength aethalometer and Scanning Mobility Particle Sizer**

An aethalometer, Model AE31 Spectrum (Manufactured by Aerosol d.o.o., Ljubljana, Slovenia) provided continuous measurements of the BC mass concentrations. The aethalometer was equipped with a  $PM_{2.5}$  impactor. The aethalometer data were recorded with a 5-minute time resolution. The optical transmission of light absorbing carbonaceous aerosol particles was measured at seven wavelengths (370, 450, 520, 590, 660, 880, and 950 nm). Measurements at 880 nm wavelength were used to determine BC mass concentration (Lavanchy et al., 1999). The aethalometer converts light attenuation measurements to BC mass using specific attenuation absorption cross-section ( $\sigma$ ) of  $16.6 \text{ m}^2 \text{ g}^{-1}$  (at 880 nm) (Aethalometer Operations manual). The default value for a near-infrared wavelength of 880 nm was set by the manufacturer. An empirical algorithm for loading effects compensation was used (Collaud Coen et al., 2010). Ångström exponent of the absorption coefficient computed by fitting an exponential curve was evaluated.

Aerosol size distribution measurements were performed using a Scanning Mobility Particle Sizer (SMPS) model 19.3.09 IFT/TT (TROPOS, Leipzig, Germany), with automatic sheath flow, temperature and relative humidity (RH) control (SMPS setup V2.6 TT 2006) as described in Wiedensohler et al. (2012) applying CPC UF-02M (Mordas et al., 2013). The measured particle size (8.7 to 840.0 nm) with a time resolution of 5 min having 72 channels.

#### 2.2.4. OC/EC, $^{14}\text{C}$ , $\delta^{13}\text{C}$ and $\delta^{15}\text{N}$ analysis

Filter measurements were performed to determine OC, EC and TC concentrations with a thermo-optical OC/EC analyser (Sunset Laboratory Inc, USA) equipped with a non-dispersive infrared (NDIR) detector. A 1.5 cm<sup>2</sup> filter punch was analysed according to the EUSAAR2 protocol (Cavalli et al., 2010). The blank filter was subtracted only from the measured OC and TC concentrations, as for the EC the corresponding blank was below the detection limits of the instruments.

$^{14}\text{C}$  in EC and TC was measured using the accelerator mass spectrometer MICADAS, equipped with a gas-capable ion source (Szidat et al., 2014).  $^{14}\text{C}$  analysis of TC was determined after combustion of filter punches in an elemental analyser, directly coupled to the MICADAS (Salazar et al., 2015). The TC  $^{14}\text{C}$  raw data were corrected for a representative field blank. For  $^{14}\text{C}$  analysis of EC, the filters were first water extracted in order to minimize charring by removing the water-soluble OC (WSOC). Then the Swiss\_4S protocol (Zhang et al., 2012) was used to remove the water-insoluble OC (WINSOC) and measure the EC  $^{14}\text{C}$ , by coupling of the Sunset instrument to the MICADAS (Agrios et al., 2015).  $^{14}\text{C}$  in OC was determined from the TC  $^{14}\text{C}$  and the EC  $^{14}\text{C}$  results with an isotope mass balance calculation. All the data from the  $^{14}\text{C}$  analysis were corrected for the decay of the  $^{14}\text{C}$  from 1950 until present. The reported uncertainty for the non-fossil fraction of EC includes both charring of OC (overestimation of EC) and EC loss (underestimation of EC) during the WINSOC removal process (Zhang et al., 2012). Non-fossil fractions of TC, EC and OC (i.e., TC<sub>nf</sub>, EC<sub>nf</sub> and OC<sub>nf</sub>) were determined from the individual  $^{14}\text{C}$  analyses and  $^{14}\text{C}$  reference values. These reference values represent emissions from purely non-fossil sources and amount  $1.06 \pm 0.03$  for TC and OC and  $1.10 \pm 0.03$  for EC based on the calculation of Mohr et al. (2009). The fossil fractions of TC, EC and OC (i.e., TC<sub>f</sub>, EC<sub>f</sub> and OC<sub>f</sub>) were determined by subtraction of the respective non-fossil fractions.

Bulk  $\delta^{13}\text{C}$  and  $\delta^{15}\text{N}$  values were derived by measuring filter pieces (1.4 cm<sup>2</sup>) wrapped in tin capsules (8\*5 mm, Elemental Microanalysis) using an elemental analyser accompanying an isotope ratio mass spectrometer (EA-IRMS, Flash EA1112—Thermo V Advantage) via a ConFlo III interface. The autosampler of the EA was continuously flushed with He (180 ml min<sup>-1</sup>) to remove all atmospheric gases. Helium flow on the oxidation column was 80 ml min<sup>-1</sup>. Flash combustion occurred in the oxidation column with the presence of O<sub>2</sub> (the O<sub>2</sub> flow was 180 ml min<sup>-1</sup> for 4 s). Formed gases were taken to the reduction column in which molecular nitrogen was obtained from any nitrogen oxides followed by a water trap

(magnesium perchlorate). The nitrogen and the carbon dioxide were separated on a packed gas chromatographic (GC) column (PoraPlot, 3m\*2cm, 35°C) and delivered to the isotope ratio mass spectrometer (via the ConFlo interface) where the measurement of carbon and nitrogen isotope ratio was made. The amount of nitrogen and carbon in the sample was determined by a thermal conductivity detector which is a part of the elemental analyser. These measurements were used in the isotope mass balance calculations (Eq. 1). The total carbon and total nitrogen fractions of the aerosol particles were used for the isotopic ratio measurements. Stable carbon and nitrogen isotopic ratio measurements were expressed relative to the Vienna Pee Dee Belemnite (VPDB) standard using the formula:

$$\delta^{13}\text{C} = \left( \frac{R_{\text{sample}}}{R_{\text{standard}}} - 1 \right) * 1000 (\text{‰}), \quad (1)$$

where  $R_{\text{sample}}$  and  $R_{\text{standard}}$  are the ratios of  $^{13}\text{C}$  to  $^{12}\text{C}$  (or  $^{15}\text{N}$  to  $^{14}\text{N}$ ) in the sample and the standard (referred to as VPDB), respectively.

Repeated analysis of certified reference material (caffeine IAEA-600) and oil (NBS 22) gave an average  $\delta^{13}\text{C}$  value: mean  $\pm \sigma = -27.77 \pm 0.08 \text{ ‰}$  (certified value: mean  $\pm \sigma = -27.771 \pm 0.043 \text{ ‰}_{\text{VPDB}}$ ) and  $\delta^{13}\text{C} = -30.031 \pm 0.043 \text{ ‰}_{\text{VPDB}}$  respectively. These values were used for  $\delta^{13}\text{C}$  measurements in order to evaluate an analytical precision and calibration of a reference gas ( $\text{CO}_2$ ) to VPDB. Meanwhile, the IAEA-600 standard gave an average  $\delta^{15}\text{N}$  value: mean  $\pm \sigma = 1 \pm 0.2 \text{ ‰}$  which was used for calibration of a reference gas ( $\text{N}_2$ ) to air (for  $\delta^{15}\text{N}$  measurements).

Stable carbon and nitrogen isotope ratios were measured in the samples with the signal intensity reaching 1000 mV or more, due to analytical restrictions (the isotope values measurements below 1000 mV did not fulfil linearity requirements of 0.07 ‰/V for the internal standard).

The mass balance equation was used to calculate the real  $\delta$  values of carbon or nitrogen of the aerosol samples (blank correction):

$$m_{\text{measured}} \times \delta X_{\text{measured}} = m_1 \times m_{\text{blank}} \times \delta X_{\text{blank}}, \quad (2)$$

where  $m_{\text{measured}}$  was the mass of measured material (carbon or nitrogen) in the measured sample,  $\delta X_{\text{measured}}$  was the measured (aerosol + filter)  $\delta$  value (carbon or nitrogen),  $m_1$  was the mass of pure material (carbon or nitrogen), and  $m_{\text{blank}}$  and  $\delta X_{\text{blank}}$  were the mass and isotope ratio (of carbon or nitrogen) of the blank filter, respectively.



### 2.2.5. Radiocarbon-based source apportionment of carbonaceous aerosols

An estimate of fossil and non-fossil primary and secondary organic carbon ( $\text{POC}_f$ ,  $\text{POC}_{nf}$ ,  $\text{SOC}_f$ ,  $\text{SOC}_{nf}$ ) was achieved by coupling ACSM-PMF results,  $^{14}\text{C}$  data, and organic marker measurements using a chemical mass balance-like approach. The sensitivity of  $\text{POC}_f$ ,  $\text{POC}_{nf}$ ,  $\text{SOC}_f$ , and  $\text{SOC}_{nf}$  contributions to the assumed parameters and measurement errors are described in details in this section. The approach is based on the  $\text{POC}_{nf}$  estimate, for a subsequent determination of  $\text{SOC}_{nf}$ ,  $\text{SOC}_f$ , and  $\text{POC}_f$  as follows:

$$\text{SOC}_{nf} = \text{OC}_{nf} - \text{POC}_{nf} \quad (3)$$

$$\text{SOC}_f = \text{SOC} - \text{SOC}_{nf} \quad (4)$$

$$\text{POC}_f = \text{OC}_f - \text{SOC}_f \quad (5)$$

$^{14}\text{C}$  measurements and ACSM-PMF results were coupled as follows. Daily  $\text{OC}_{nf}$  measurements from radiocarbon analysis as well as average daily POA from ACSM-PMF results provided two upper boundaries for the daily  $\text{POC}_{nf}$  contribution. In this manner we identified a possible daily range of  $\text{POC}_{nf}$  contributions. In order to determine more precisely the  $\text{POC}_{nf}$  daily contributions within the aforementioned possible daily ranges, we performed a sensitivity analysis. Briefly, in the sensitivity analysis we considered a uniform distribution of possible  $\text{POC}_{nf}$  contributions within the identified possible daily ranges, meaning that each  $\text{POC}_{nf}$  value in the selected ranges was considered as equally probable (however, as discussed in the next section, in order to explore the influence of this assumption we also performed the same sensitivity analysis assuming a non-uniform distribution). Assuming no  $\text{POC}_{nf}$  contribution from other sources than BBOC, each  $\text{POC}_{nf}$  contribution in the acceptable daily ranges could be written either as  $[\text{BBOC}] = [\text{levoglucosan}]/\alpha$  or as  $[\text{BBOC}] = [\text{EC}_{nf}]/\beta$ , where  $\alpha$  represents the levoglucosan/BBOC ratio and  $\beta$  represents the  $\text{EC}_{nf}$ /BBOC ratio. In two separated sensitivity analyses we scanned broad  $\alpha$  and  $\beta$  ranges covering the possible  $\text{POC}_{nf}$  daily ranges and we retained only  $\text{POC}_{nf}$ ,  $[\text{levoglucosan}]/\alpha$ , and  $[\text{EC}_{nf}]/\beta$  combinations associated to selected acceptance criteria described in the following. From the acceptable solutions we then derived the daily probability distribution function of  $\text{POC}_f$ ,  $\text{SOC}_{nf}$ ,  $\text{SOC}_f$ ,  $\text{POC}_f$ ,  $\alpha$ , and  $\beta$ .

The assumption that each input  $\text{POC}_{nf}$  contribution in the selected possible range is equally probable (hereafter referred to as “uniform distribution approach”) has advantages and

drawbacks: while this assumption doesn't consider any a priori information about levoglucosan/ $\text{POC}_{\text{nf}}$  and  $\text{EC}_{\text{nf}}/\text{POC}_{\text{nf}}$ , it considers those ratios as equally possible. To explore the influence of this assumption on our results we performed the same sensitivity analysis assuming an input levoglucosan/ $\text{POC}_{\text{nf}}$  distribution derived from 33 profiles for combustion of hard or softwoods in domestic fireplaces or woodstoves (Fine et al. 2001, 2002, 2004a, 2004b, Schmidl et al. 2008, the approach is hereafter referred to as “non-uniform distribution approach”). We eventually derived the probability distribution functions of the levoglucosan/ $\text{POC}_{\text{nf}}$  and  $\text{EC}_{\text{nf}}/\text{POC}_{\text{nf}}$  ratios relative to the acceptable solutions. The two approaches provided similar results. From the uniform distribution approach, a median levoglucosan/ $\text{POC}_{\text{nf}}$  ratio of 0.18 (1<sup>st</sup> quartile = 0.14; 3<sup>rd</sup> quartile = 0.23) and a median  $\text{EC}_{\text{nf}}/\text{POC}_{\text{nf}}$  ratio of 0.32 (1<sup>st</sup> quartile = 0.28; 3<sup>rd</sup> quartile = 0.36) were retrieved, whilst from the non-uniform distribution approach a median levoglucosan/ $\text{POC}_{\text{nf}}$  ratio of 0.15 (1<sup>st</sup> quartile = 0.13; 3<sup>rd</sup> quartile = 0.18) and a median  $\text{EC}_{\text{nf}}/\text{POC}_{\text{nf}}$  ratio of 0.33 (1<sup>st</sup> quartile = 0.28; 3<sup>rd</sup> quartile = 0.36) were obtained.

In the following section a technical description of the sensitivity analysis implementation is reported. For each filter sample  $i$ , 10000 random combinations (r) of input data,  $[\text{TC}]_{i,r}$ ,  $[\text{EC}]_{i,r}$ ,  $[\text{EC}_{\text{f}}]_{i,r}$ , and  $[\text{Levoglucosan}]_{i,r}$ , were generated. In this process, we assume a normal distribution of the errors around the average  $[X]_i$  value (X being one of the input values mentioned above), and a distribution width equal to the standard deviation  $\sigma[X]_i$ :

For each random combination of input data, the corresponding  $[\text{OC}]_{i,r}$ ,  $[\text{EC}_{\text{nf}}]_{i,r}$ , and  $[\text{OC}_{\text{nf}}]_{i,r}$  values were determined as:

$$[\text{OC}]_{i,r} = [\text{TC}]_{i,r} - [\text{EC}]_{i,r}, \quad (6)$$

$$[\text{EC}_{\text{nf}}]_{i,r} = [\text{EC}]_{i,r} - [\text{EC}_{\text{f}}]_{i,r}, \quad (7)$$

$$[\text{OC}_{\text{nf}}]_{i,r} = [\text{OC}]_{i,r} - [\text{OC}_{\text{f}}]_{i,r}. \quad (8)$$

10000 random  $[\text{SOC}]_s$  values were generated by randomly selecting a daily average  $[\text{SOA}]_s$  value from one of the 20 ACSM-PMF runs (s). The corresponding  $[\text{SOC}]_s$  values were derived as:

$$[\text{SOC}]_s = [\text{SOA}]_s / (\text{OM}/\text{OC})_{\text{SOA}(s)} \quad (9)$$

$(\text{OM}/\text{OC})_{\text{SOA}(s)}$  and  $\sigma(\text{OM}/\text{OC})_{\text{SOA}(s)}$  were calculated according to Aiken et al., 2009 as function of the fractional contribution of the  $m/z$  44 ( $f_{44}$ ) to the  $\text{SOA}_s$  mass spectra. Fröhlich et al. (2015) showed a systematic difference between  $f_{44}$  measured from ACSM and AMS,

therefore an empirical correction factor was accordingly applied to rescale  $f44$  from ACSM ( $f44_{\text{ACSM}}$ ) data to the corresponding AMS  $f44$  value ( $f44_{\text{AMS}}$ ). The uncertainty relative to the  $f44$  correction factor was propagated into  $\sigma(\text{OM/OC})_{\text{SOA(s)}}$  which includes the  $\text{O/C}_s$  uncertainty as well. Each  $[\text{SOC}]_{i,r}$  value was obtained by randomly varying  $[\text{SOC}]_s$  assuming a normal distribution of errors around the average value  $[\text{SOC}]_s$  and a distribution width equals  $\sigma(\text{OM/OC})_{\text{SOA(s)}}$ .  $[\text{BBOC}]_{i,r}$  contributions for each sample  $i$  were derived as follows:

$$[\text{BBOC}]_{i,r} = [\text{levoglucosan}]_{i,r}/\alpha, \quad (10)$$

$$[\text{BBOC}]_{i,r} = [\text{EC}_{\text{nf}}]_{i,r}/\beta, \quad (11)$$

where  $\alpha$  represents the levoglucosan/BBOC ratio. This ratio was systematically varied between 0.01 and 0.31 according to Huang et al. (2014) and references therein (scan step equals 0.01).  $\beta$  corresponds to the EC/BBOC ratio. Values of  $\beta$  were systematically varied between 0.1 and 0.4 according to Zhang et al. (2015) and references therein (scan step equals 0.01). 10000  $[\text{BBOC}]_{i,r,\alpha}$  and 10000  $[\text{BBOC}]_{i,r,\beta}$  were determined as in Eq. (8) and (9). Only acceptable  $[\text{BBOC}]_{i,r,\alpha/\beta}$  ( $= [\text{POC}_{\text{nf}}]_{i,r,\alpha/\beta}$ ) values were considered for the sensitivity analysis. The criteria to consider a  $[\text{BBOC}]_{i,r,\alpha/\beta}$  value as acceptable were:

$$\text{a) } [\text{BBOC}]_{i,r,\alpha/\beta} \leq [\text{POC}]_{i,r} \text{ and b) } [\text{BBOC}]_{i,r,\alpha/\beta} \leq [\text{OC}_{\text{nf}}]_{i,r} \quad (12)$$

$[\text{POC}]_{i,r}$  was determined as follows:

$$[\text{POC}]_{i,r} = [\text{OC}]_{i,r} - [\text{SOC}]_{i,r}, \quad (13)$$

Only acceptable  $[\text{POC}]_{i,r}$  values were considered. The criterion to consider a  $[\text{POC}]_{i,r}$  value as acceptable was:

$$\text{c) } [\text{POA}]_s/[\text{POC}]_{i,r} \geq 1.3 \text{ according to Mohr et al. (2009), Aiken et al. (2009).}$$

$[\text{SOC}_{\text{nf}}]_{i,r}$  values were then derived as:

$$[\text{SOC}_{\text{nf}}]_{i,r} = [\text{OC}_{\text{nf}}]_{i,r} - [\text{POC}_{\text{nf}}]_{i,r} \quad (14)$$

Only acceptable  $[\text{SOC}_{\text{nf}}]_{i,r}$  values were considered, where

$$\text{d) } [\text{SOC}_{\text{nf}}]_{i,r} \leq [\text{SOC}]_{i,r} \quad (15)$$

Only solutions where all 4 criteria a), b), c), and d) held were considered acceptable and retained.

Finally,  $[\text{SOC}_f]_{i,r}$  and  $[\text{POC}_f]_{i,r}$  were calculated as:

$$[\text{SOC}_f]_{i,r} = [\text{SOC}]_{i,r} - [\text{SOC}_{\text{nf}}]_{i,r}, \quad (16)$$

$$[\text{POC}_f]_{i,r} = [\text{OC}_f]_{i,r} - [\text{SOC}_f]_{i,r}. \quad (17)$$

## 2.2.6. Satellite products and organic markers

Determination of organic marker concentrations were performed using developed in-situ derivatization thermal desorption gas chromatography time of flight mass spectrometry (IDTD-GC-MS) method (Orasche et al., 2011).

Biomass burning episodes were explored using a variety of remote sensing datasets and their derived properties. Satellite data and ground based observations of aerosol properties from the MODIS, HYSPLIT and SILAM (Sofiev et al., 2006) were coupled to analyse the variability of carbonaceous aerosols in Lithuania (Fig. 2).

The MODIS sensors on-board NASA's Terra and Aqua satellites provides multiple thermal observations of the Earth on 9–10 March 2014 at a spatial resolution of 1 km using the latest version of the MODIS Active Fire Product (MOD14/MYD14) algorithm (MODIS, 2011). To identify the influence of air masses from different transport pathways on the large BB event occurring at Preila, 72-h back trajectories at an arrival height of 100, 200 and 500 m were calculated by Hybrid Single Particle Lagrangian Integrated Trajectory (HYSPLIT) Model Version 4.8. All air mass back trajectories were generated using Gridded Meteorological Data archives of the Air Resource Laboratory (ARL), National Ocean and Atmospheric Administration (NOAA) (Fig. 2A).

The Navy Aerosol Analysis and Prediction System (NAAPS) model results were used to define the distribution of BB aerosols from wildfires area (model description and results are available from the web pages of the Naval Research Laboratory, Monterey, CA, USA; <http://www.nrlmry.navy.mil/aerosol/>) (Fig. 2B). The NAAPS model has been adapted to combine real-time observations of biomass burning based on the joint Navy/NASA/NOAA Fire Locating and Modelling of Burning Emissions system (FLAMBE, <http://www.nrlmry.navy.mil/flambe/>) (Reid et al., 2004). The method has proven helpful in previous studies of long-range and regional transport of smoke (Honrath et al., 2004). The resolution of 2.5° longitude × 2.5° latitude National Centers for Environmental Prediction (NCEP) reanalysis data (Kanamitsu et al., 2002) during grass burning episode were analysed to illustrate the sub synoptic-scale weather feature among the biomass burning events over Lithuania issued every 6 h for March 2014 (Fig. 2C). SILAM is an air quality and emergency open code system (<http://silam.fmi.fi/>) providing PM<sub>2.5</sub> emission maps by Eulerian dynamics and a combination of basic acid and ozone chemistry with inert particles for fire and

anthropogenic primary PM emission to account for the fire induced aerosol contribution (Fig. 2D).

## Results and discussion

### 2.1 Identification of grass burning event

Massive active fires occurred throughout the Kaliningrad region (Russia), Belorussia and Ukraine (Fig. 2A) when a high atmospheric pressure system was situated over the study area, as illustrated in the weather map of Fig. 2C. The plumes from those fires covered a large area south of the Baltic region and were transported thousands of kilometres downwind affecting the background air in Lithuania (Fig. 2). Although the number of fires was similar to that one of previous years, the impact of the fire events on the Lithuanian air quality was enhanced in March 2014 due to air mass transport of smoke entrained in deep convection by the large scale circulation around the pressure maximum of the anticyclonic system (Fig. 2C). This is consistent with the relatively high concentrations of smoke reaching Preila as predicted by NAAPS (Fig. 2B).

The weather maps showed that the high concentration of pollutants during this BB event was caused by the anticyclonic large-scale movement, which persisted throughout the lower troposphere causing stagnant conditions and extended aerosol residence time.

### 2.2 Investigation of PM<sub>1</sub> composition and ambient concentrations of organic tracers

The climatic conditions in West Europe as well as in west part of Lithuania are particular, as the moderate warm climate dominating by air mass transport from Atlantic Ocean, leading to higher humidity. Annual mean temperature increases in west-east direction. The average temperature of March was ~3–4 °C. During the BB event (9–11 March) combustion products were spread over the study region by the large-scale atmospheric circulation processes. At the beginning of the BB episode, the wind speed was up to 3 m s<sup>-1</sup> on average in the daytime of 9<sup>th</sup> March, causing weaker dilution of the pollutants while the BC concentration were higher than 12 µg m<sup>-3</sup>.

During the campaign on average organic aerosol (46 %, 3.2 µg m<sup>-3</sup> ( $\sigma$  = 4.8 µg m<sup>-3</sup>)) constituted the major fraction of the NR-PM<sub>1</sub> aerosol concentration composition measured by ACSM with lower contributions of sulfate (17 %, 1.2 µg m<sup>-3</sup> ( $\sigma$  = 1.1 µg m<sup>-3</sup>)), nitrate (20 %, 1.2 µg m<sup>-3</sup> ( $\sigma$  = 1.1 µg m<sup>-3</sup>)).

1 1.4  $\mu\text{g m}^{-3}$  ( $\sigma = 1.8 \mu\text{g m}^{-3}$ ), ammonium (15 %, 1.0  $\mu\text{g m}^{-3}$  ( $\sigma = 0.9 \mu\text{g m}^{-3}$ )), and chloride  
2 (2 %, 0.1  $\mu\text{g m}^{-3}$  ( $\sigma = 0.3 \mu\text{g m}^{-3}$ )). The average composition of NR-PM<sub>1</sub> showed similar  
3 dominance of organics to previous observations in Europe (e.g. Crippa et al., 2014). OA  
4 contribution to NR-PM<sub>1</sub> was found to be much higher during the grass burning period (61 %,   
5 8.6  $\mu\text{g m}^{-3}$  ( $\sigma = 5.0 \mu\text{g m}^{-3}$ )), followed by sulfate (5 %, 1.4  $\mu\text{g m}^{-3}$  ( $\sigma = 0.5 \mu\text{g m}^{-3}$ )), nitrate  
6 (19 %, 3.0  $\mu\text{g m}^{-3}$  ( $\sigma = 1.4 \mu\text{g m}^{-3}$ )), ammonium (13 %, 1.6  $\mu\text{g m}^{-3}$  ( $\sigma = 0.7 \mu\text{g m}^{-3}$ )), and  
7 chloride (3 %, 0.4  $\mu\text{g m}^{-3}$  ( $\sigma = 0.3 \mu\text{g m}^{-3}$ )) (Fig. 5A).

8 Quantification of monosaccharide anhydrides together with OC and EC are presented in Fig.  
9 3. It is evident that during the event, when grass burning was most intense, the levoglucosan  
10 concentration increased up to 680  $\text{ng m}^{-3}$ . That was significantly lower than values reported  
11 during extreme event of August 2010 in Moscow – 3100  $\text{ng m}^{-3}$  (Popovicheva et al., 2014)  
12 and are higher than values (220–290  $\text{ng m}^{-3}$ ) reported during a major biomass burning  
13 episode over northern Europe in Helsinki (Saarikoski et al., 2007), while background values  
14 in Nordic rural background sites were found to be 2.1–9.8  $\text{ng m}^{-3}$  (Yttri et al., 2011).  
15 Concentrations of mannosan varied from 3.1 to 68.0  $\text{ng m}^{-3}$ , with a mean value of 19.0  $\text{ng m}^{-3}$ ,  
16 and concentrations of galactosan varied from 1.0 to 12.0  $\text{ng m}^{-3}$ . Concentrations of  
17 mannosan varied from 3.1 to 68.0  $\text{ng m}^{-3}$  and those of galactosan from 1.0 to 12.0  $\text{ng m}^{-3}$ .  
18 The levoglucosan to mannosan (L/M), levoglucosan to galactosan (L/G) and levoglucosan to  
19 OC (L/OC) ratios were used before to separate different BB sources (Fabbri et al., 2009;  
20 Oanh et al., 2011; Harrison et al., 2012). We measured average L/M and L/G ratios of 16.4  
21 and 135.8, respectively. This is similar to the values found by Orasche et al. (2012) from  
22 wood combustion in residential wood appliances and in the range of L/M ratios reported (2.0–  
23 33.3) for grass fires by Oros et al. (2006). Excluding the strong event days of March 9 and 10  
24 the sugars showed a good correlation with each other ( $R^2 > 0.86$ ). On March 9 and 10 the  
25 mannosan/galactosan was lower at 2–6, indicating different source contribution to the other  
26 days. Low mannosan/galactosan ratios were observed for grass and leaves (Sullivan, May et  
27 al. 2014). We observed an L to OC ratio from 0.06 to 0.16 during the biomass burning period  
28 and of  $\sim 0.03$  during the days without biomass burning events. The values observed during  
29 biomass burning are in the range of those (0.04–0.20) reported for wildland fuels (Sullivan et  
30 al. 2008). The OC/EC ratio ranged from 1.5 to 6.2 being lower on event days (2.4–3.0)  
31 indicating an aerosol composition dominated by organic aerosol. During the intensive grass  
32 burning episode, consecutive new particle formation (NPF) episodes were observed.

Observed NPF could be attributed to the grass burning and secondary biomass burning product transformation as was evaluated in earlier studies over same area (Ulevicius et al., 2010b). At 13:00, there was a significant new particle formation on 9<sup>th</sup> and 10<sup>th</sup> March followed by subsequent growth up to three hours. The total particle number concentration with a daily mean value of 6440 cm<sup>-3</sup> (with maximum value of 13000 cm<sup>-3</sup>), which was extremely much higher than the daily mean observations in non-event days (1660 cm<sup>-3</sup>). In this area annual total particle concentration of 2650 cm<sup>-3</sup> was observed (Byčenkienė et al., 2013). Non-event day was characterized by bimodal (Aitken (geometric mean diameter ( $D_g$ ) of 44 nm) and accumulation ( $D_g$  = 128 nm)) modes with a standard deviation of 1.68 and 1.87, respectively. In comparison, during biomass burning event trimodal (nucleation ( $D_g$  = 9.0 nm), Aitken ( $D_g$  = 31.0 nm) and accumulation ( $D_g$  = 102 nm) modes with a standard deviation of 1.77, 1.71 and 1.68, respectively. However volume distribution was characterized by bimodal size distribution for non-event day ( $D_g$  = 330 and 665 nm) and event day ( $D_g$  = 250 and 590 nm).

The measured  $\delta^{13}\text{C}$  values varied from -28.2 to -26.7 ‰. The lowest stable carbon isotope ratio values (-28.5 ‰) were detected during the period with the highest total carbon concentration of 12.2  $\mu\text{g m}^{-3}$  (2014.03.10) and 8.5  $\mu\text{g m}^{-3}$  (2014.03.09). The highest concentration 14.0  $\mu\text{g m}^{-3}$  of nitrogen was detected on 10 March 2014. The nitrogen isotope ratio values varied from +1.0 to +13.0 ‰ (Fig. 4).

Stable carbon and nitrogen isotope ratios values of aerosol particles derived from biomass burning (C3 plants) and liquid fossil fuel are overlapping (Garbaras et al., 2015, Masalaite et al., 2015, Turekian et al., 1998). Coal derived aerosol particles are characterised by higher  $\delta^{13}\text{C}$  and lower  $\delta^{15}\text{N}$  values (Fig. 4, solid lines).  $\delta^{13}\text{C}$  values of aerosol particles during wild grass burning events distinguish in low  $\delta^{13}\text{C}$  values (Garbaras et al. 2008, Ulevicius et. al. 2010b). The above mentioned distribution of  $\delta^{13}\text{C}$  and  $\delta^{15}\text{N}$  values allowed excluding coal burning as main source for aerosol particles at Preila during the investigated event. Aerosol particles with the  $\delta^{13}\text{C}$  values equal -28 ‰ and below originated mainly from grass burning events. This interpretation of the data is consistent with the radiocarbon analysis shown below.

### 2.3 Source apportionment of EC and OC using $^{14}\text{C}$ data

Relative fossil and non-fossil contributions to OC and EC were evaluated using  $^{14}\text{C}$  analysis (Szidat et al., 2014) to enable a more detailed source attribution of the carbonaceous

aerosol mass. Widely used, two-source simple models (Currie, 2000; Lemire et al., 2002; Lewis et al., 2004; Szidat et al., 2004) can only distinguish fossil from non-fossil TC emissions. Here, carbonaceous aerosol was described to be composed of the following categories:  $OC_f$  and  $EC_f$  attributed to primary and secondary fossil fuel combustion; and  $OC_{nf}$ , and  $EC_{nf}$  typically emitted by to primary and secondary biomass burning, cooking, biogenic emissions and non-fossil OC combustion (Table 2, Fig. 5). There was day-to-day variation in the fractional contributions to TC throughout the BB event. The fraction of elemental carbon from biomass burning  $EC_{bb}$  ( $= EC_{nf}$ ) to total EC was found to be on average  $67 \pm 3$  %. For  $EC_{bb}$  the mean relative contribution to total carbon in background areas of Northern countries was found to be  $< 1.5$  % on non-event days (Yttri et al., 2011). It was also reported that a major peak in  $EC_{bb}$  values between March and April was observed at the Zeppelin atmospheric observatory (Yttri et al. 2014). Such high values are unusual and have only been found in wood burning dominated places like villages in Alpine valleys (Zotter et al., 2014). This shows, together with high levels of levoglucosan, that biomass burning contributed to a large extent to  $OC_{nf}$  during this event. A mean light absorption coefficient  $\alpha_{370-950}$  (the absorption exponent calculated using the seven Aethalometer wavelengths) of 1.38 ( $\sigma = 0.11$ ) was obtained during wildfires, which is higher than the mean  $\alpha_{370-950}$  calculated for the non-event days (1.13,  $\sigma = 0.19$ ). The light absorption exponent values were calculated with  $\lambda = 370 - 520$  nm and  $\lambda = 590 - 950$  nm wavelengths for comparison purpose. The mean values of  $\alpha_{370-520}$  and  $\alpha_{590-950}$  were found to be 1.53 ( $\sigma = 0.19$ ) and 1.32 ( $\sigma = 0.09$ ) during event day and 1.25 ( $\sigma = 0.27$ ) and 1.13 ( $\sigma = 0.18$ ) during non-event days, respectively. In comparison during the same event in Preila higher mean values of  $\alpha_{370-520}$  and  $\alpha_{590-950}$  nm were observed (2.4 ( $\sigma = 0.1$ ) and 1.5 ( $\sigma = 0.1$ , respectively)) in 2008, as well as during the event in 2009 (2.3 ( $\sigma = 0.1$ ) and 1.6 ( $\sigma = 0.1$ , respectively)) (Ulevicius et al., 2010). This is an indication of influence of the biomass burning on the Ångström exponent of the absorption coefficient  $\alpha$ . The impact of organic aerosols on the spectral dependence of light absorption was early confirmed by OC/EC ratios. PMF analysis of OA spectra resolved two OA components, which are attributed to POA and SOA, whose mass spectra and time series are presented in Fig. 5 B, C. Combining these results with the  $^{14}C$  measurements as described in section 2.2.4 shows that the high grass burning pollution event is characterized by a high non-fossil organic compound fraction, which accounts for up to  $\sim 90$  % of total carbon mass.



SOA showed reasonable correlation ( $R^2 = 0.62$ ) with average  $\text{NH}_4^+$  mass concentration during the BB event.  $\text{NH}_4^+$  is in this case a good tracer for secondary aerosol, as it correlates well with the sum of  $\text{NO}_3^-$  and  $\text{SO}_4^{2-}$  ( $R^2 = 0.96$ ; linear fit:  $y = 0.816x + 0.005$ ) (Fig. 6). There was day-to-day variation throughout the study period with the non-fossil contribution to organic carbon between 67–86 %.  $\text{OC}_{\text{nf}}$  was estimated to be ~65 % primary, while the primary fraction of the  $\text{OC}_{\text{f}}$  in Preila was estimated to be ~93 %. Conversely, when  $\text{EC}_{\text{f}}$  showed a lower contribution (2014.03.07 and 2014.03.10; 26 % and 24 %, respectively),  $\text{OC}_{\text{f}}$  was also lower (15 %) (Table 3). The high fraction of biomass burning was corroborated by measurements of levoglucosan. Other molecular markers such as hopanes for traffic emissions and picene for coal combustion (Rutter et al., 2009) were also measured in order to monitor the possible contribution of fossil fuel combustion during the high pollution event. Although their concentrations increased during the episode, suggesting a contribution of co-transported fossil fuel combustion aerosols, the radiocarbon analysis revealed the contribution of this fraction to be minor ( $\text{EC}_{\text{f}}$  ranged from 0.3 to 1.1;  $\text{OC}_{\text{f}}$  ranged from 0.5 to 1.6 (Fig. 5). Values of molecular markers are provided in Table 1 of the Supplementary material. The combination of both techniques allowed a better characterization of the carbonaceous aerosol sources. POA determined with the ACSM is mostly non-fossil and originates from grass burning. The lines in Fig. 7 represent the absolute contribution of each source during 5–10 March 2014. It is shown that  $\text{POC}_{\text{nf}}$  and  $\text{SOC}_{\text{nf}}$  concentrations increase drastically (from 1.1 to  $5.4 \mu\text{g m}^{-3}$  for  $\text{POC}_{\text{nf}}$ ; from 0.9 to  $3.1 \mu\text{g m}^{-3}$  for  $\text{SOC}_{\text{nf}}$ ) with increasing influence of biomass burning, whereas the concentrations of the respective fossil fractions show a smaller increase during this episode. From the acceptable solutions obtained from the sensitivity test described in section 2.2.7, we derived the probability distribution functions of the different daily contributions for  $\text{POC}_{\text{f}}$ ,  $\text{SOC}_{\text{nf}}$ ,  $\text{SOC}_{\text{f}}$ ,  $\text{POC}_{\text{f}}$  fractions (Fig. 7). The median Levoglucosan/BBOC and EC/BBOC ratios obtained from the sensitivity tests is consistent with values reported in Zhang et al. (2015) and Huang et al. (2014) (Fig. 8).

In Zhang et al. (2015) agricultural waste combustion is considered to be the main contributor to the total biomass burning. Note that on 5 March a different Levoglucosan/BBOC ratio was found (0.31) compared to the non-event days (~0.15). Also, this is consistent with different wind back-trajectories, associated to air masses originating in the Southern and Central Russian Federal districts, i.e. air masses with a different geographical origin and associated to potentially different types of biomass burning.

### 3 Conclusions

In March 2014, an intensive field campaign was conducted in the marine background of South Eastern Baltic region during a period of intensive grass burning. This paper provides the biomass burning related aerosol concentrations during grass burning estimated by data that stem from a synthesis of various techniques including surface online/ offline and satellite based measurements. Lidar vertical profiles allowed confirming smoke plume from wild fire regions. Levels of source specific tracers, i.e, levoglucosan as well as  $^{14}\text{C}$  of TC, EC and OC have been used as input for source apportionment of the carbonaceous aerosol approach. Overall, EC and OC were dominated by non-fossil sources. The total POC fraction was separated into  $\text{POC}_f$  and  $\text{POC}_{nf}$ . In term of OC mass,  $\text{POC}_{nf}$  contributes on average 56 %, while relative contribution to TC was found to be on average 39 %. In case of SOC, the contribution of  $\text{OC}_f$  reached on average 10.3 % (non-fossil – 25 %). The  $\delta^{13}\text{C}$  value of -28.5 % indicated the dominance of the aerosol derived from the vegetation burning as no significant carbon isotope fractionation occurs between the aerosol particles from biomass burning and the raw biomass material.

### Acknowledgements

This work was supported by the Lithuanian-Swiss Cooperation Programme “Research and Development” project AEROLIT (Nr. CH-3-ŠMM-01/08).

## References

- Agrios, K., Salazar, G. A., Zhang, Y. L., Uglietti, C., Battaglia, M., Luginbühl, M., Ciobanu, V. G., Vonwiller, M., and Szidat, S.: Online coupling of pure O<sub>2</sub> thermo-optical methods - <sup>14</sup>C AMS for source apportionment of carbonaceous aerosols study, *Nucl. Instrum. Meth. Phys. Res. B.*, 361, 288-293, doi:10.1016/j.nimb.2015.06.008, 2015.
- Aiken, A. C., Salcedo, D., Cubison, M. J., Huffman, J. A., DeCarlo, P. F., Ulbrich, I. M., Docherty, K. S., Sueper, D., Kimmel, J. R., Worsnop, D. R., Trimborn, A., Northway, M., Stone, E. A., Schauer, J. J., Volkamer, R. M., Fortner, E., de Foy, B., Wang, J., Laskin, A., Shutthanandan, V., Zheng, J., Zhang, R., Gaffney, J., Marley, N. A., Paredes-Miranda, G., Arnott, W. P., Molina, L. T., Sosa, G., and Jimenez, J. L.: Mexico City aerosol analysis during MILAGRO using high resolution aerosol mass spectrometry at the urban supersite (T0) – Part 1: Fine particle composition and organic source apportionment, *Atmos. Chem. Phys.*, 9, 6633– 6653, doi:10.5194/acp-9-6633-2009, 2009.
- Akagi, S. K., Craven, J. S., Taylor, J. W., McMeeking, G. R., Yokelson, R. J., Burling, I. R., Urbanski, S. P., Wold, C. E., Seinfeld, J. H., Coe, H., Alvarado, M. J., and Weise, D. R.: Evolution of trace gases and particles emitted by a chaparral fire in California, *Atmos. Chem. Phys.*, 12, 1397–1421, doi:10.5194/acp-12-1397-2012, 2012.
- Baldini, G., Campadelli, P., and Fradegrada, M.: Biomass burning monitoring by scene analysis, In *Proceedings of Visualization, Imaging, and Image Processing*, Calgary, 2002.
- Baron, P. A. and Willeke, K. (Eds.): *Aerosol Measurement: Principles, Techniques, and Applications* 2nd Edition, Wiley, New York, 2001.
- Beddows, D. C. S., Dall'Osto, M., Harrison, R. M., Kulmala, M., Asmi, A., Wiedensohler, A., Laj, P., Fjaeraa, A. M., Sellegri, K., Birmili, W., Bukowiecki, N., Weingartner, E., Baltensperger, U., Zdimal, V., Zikova, N., Putaud, J.-P., Marinoni, A., Tunved, P., Hansson, H.-C., Fiebig, M., Kivekäs, N., Swietlicki, E., Lihavainen, H., Asmi, E., Ulevicius, V., Aalto, P. P., Mihalopoulos, N., Kalivitis, N., Kalapov, I., Kiss, G., de Leeuw, G., Henzing, B., O'Dowd, C., Jennings, S. G., Flentje, H., Meinhardt, F., Ries, L., Denier van der Gon, H. A. C., and Visschedijk, A. J. H.: Variations in tropospheric submicron particle size distributions across the European continent 2008–2009, *Atmos. Chem. Phys.*, 14, 4327-4348, doi:10.5194/acp-14-4327-2014, 2014.

1 Bougiatioti, A., Stavroulas, I., Kostenidou, E., Zarnmpas, P., Theodosi, C., Kouvarakis, G.,  
2 Canonaco, F., Prévôt, A. S. H., Nenes, A., Pandis, S. N., and Mihalopoulos, N.: Processing of  
3 biomass-burning aerosol in the eastern Mediterranean during summertime, *Atmos. Chem.*  
4 *Phys.*, 14, 4793-4807, doi:10.5194/acp-14-4793-2014, 2014.

5 Byčenkienė, S., Ulevicius, V., and Kecorius, S.: Characteristics of black carbon aerosol mass  
6 concentration over the East Baltic region from two-year measurements, *J. Environ. Monit.*,  
7 13(4), 1027–1038, doi: 10.1039/C0EM00480D, 2011.

8 Byčenkienė, S., Ulevicius V., Dudoitis V., and Pauraitė J.: Identification and characterization  
9 of black carbon aerosol sources in the East Baltic region, *Adv. Meteor.*, 2013, Article ID  
10 380614, doi.org/10.1155/2013/380614, 2013.

11 Canonaco, F., Crippa, M., Slowik, J. G., Baltensperger, U., and Prevot A. S. H.: SoFi, an  
12 IGOR-based interface for the efficient use of the generalized multilinear engine (ME-2) for  
13 the source apportionment: ME-2 application to aerosol mass spectrometer data, *Atmos. Meas.*  
14 *Tech.*, 6(12), 3649-3661, 2013.

15 Capes, G., Johnson, B., McFiggans, G., Williams, P. I., Haywood, J., and Coe, H.: Aging of  
16 biomass burning aerosols over West Africa: aircraft measurements of chemical composition,  
17 microphysical properties, and emission ratios, *J. Geophys. Res. Atmos.*, 113, D00C15, doi:  
18 10.1029/2008JD009845, 2008.

19 Cavalli, F., Viana, M., Yttri, K. E., Genberg, J., and Putaud, J.-P.: Toward a standardised  
20 thermal-optical protocol for measuring atmospheric organic and elemental carbon: the  
21 EUSAAR protocol, *Atmos. Meas. Tech.*, 3, 79–89, doi:10.5194/amt-3-79-2010, 2010.

22 Ceburnis, D., Garbaras, A., Szidat, S., Rinaldi, M., Fahrni, S., Perron, N., Wacker, L., Leinert,  
23 S., Remeikis, V., Facchini, M. C., Prevot, A. S. H., Jennings, S. G., O'Dowd, C. D.:  
24 Quantification of the carbonaceous matter origin in submicron marine aerosol particles by  
25 dual carbon isotope analysis, *Atmos. Chem. Phys.*, 11, 8593-8606, doi:10.5194/acp-11-8593-  
26 2011.

27 Collaud Coen, M., Weingartner, E., Apituley, A., Ceburnis, D., Fierz-Schmidhauser, R.,  
28 Flentje, H., Henzing, J. S., Jennings, S. G., Moerman, M., Petzold, A., Schmid, O., and  
29 Baltensperger, U.: Minimizing light absorption measurement artifacts of the Aethalometer:  
30 evaluation of five correction algorithms, *Atmos. Meas. Tech.*, 3, 457–474, doi: 10.5194/amt-  
31 3-457-2010, 2010.

1 Crippa, M., Canonaco, F., Lanz, V. A., Äijälä, M., Allan, J. D., Carbone, S., Capes, G.,  
2 Ceburnis, D., Dall'Osto, M., Day, D. A., DeCarlo, P. F., Ehn, M., Eriksson, A., Freney, E.,  
3 Hildebrandt Ruiz, L., Hillamo, R., Jimenez, J. L., Junninen, H., Kiendler-Scharr, A.,  
4 Kortelainen, A.-M., Kulmala, M., Laaksonen, A., Mensah, A. A., Mohr, C., Nemitz, E.,  
5 O'Dowd, C., Ovadnevaite, J., Pandis, S. N., Petäjä, T., Poulain, L., Saarikoski, S., Sellegri, K.,  
6 Swietlicki, E., Tiitta, P., Worsnop, D. R., Baltensperger, U., and Prévôt, A. S. H.: Organic  
7 aerosol components derived from 25 AMS data sets across Europe using a consistent ME-2  
8 based source apportionment approach, *Atmos. Chem. Phys.*, 14, 6159-6176, doi:10.5194/acp-  
9 14-6159-2014, 2014.

10 Crutzen, P. J., Heidt, L. E., Krasnec, J. P., Pollock, W. H., and Seiler, W.: Biomass burning as  
11 a source of atmospheric gases CO, H<sub>2</sub>, N<sub>2</sub>O, NO, CH<sub>3</sub>Cl, and COS, *Nature* 282, 253-256,  
12 doi:10.1038/282253a0, 1979.

13 Currie, L. A.: Evolution and multidisciplinary frontiers of <sup>14</sup>C aerosol science, *Radiocarbon*  
14 42, 115–126, 2000.

15 Davison, A. C. and Hinkley, D. V.: *Bootstrap Methods and Their Application*, Cambridge  
16 University Press, Cambridge, UK, 582 pp., 1997.

17 Fabbri, D., Torri, C., Simoneit, B., Marynowski, L., Rushdi, A., Fabianska, M.: Levoglucosan  
18 and other cellulose and lignin markers in emissions from burning of Miocene lignites, *Atmos.*  
19 *Environ.*, 43, 2286-2295, doi:10.1016/j.atmosenv.2009.01.030, 2009.

20 Fine, P. M., Cass, G. R., Simoneit, B. R. T.: Chemical characterization of fine particle  
21 emissions from fireplace combustion of woods grown in the northeastern United States,  
22 *Environ. Sci. Technol.*, 35, 2665-2675, doi:10.1021/es001466k, 2001.

23 Fine, P. M., Cass, G. R., Simoneit, B. R. T.: Chemical characterization of fine particle  
24 emissions from the fireplace combustion of woods grown in the southern United States.  
25 *Environ. Sci. Technol.*, 36, 1442-1451, doi: 10.1021/es0108988, 2002.

26 Fine, P. M., Cass, G. R., Simoneit, B. R. T.: Chemical characterization of fine particle  
27 emissions from the wood stove combustion of prevalent United States tree species. *Environ.*  
28 *Eng. Sci.*, 21, 705-721, doi: 10.1089/ees.2004.21.705, 2004a.

1 Fine, P. M., Cass, G. R., Simoneit, B. R. T.: Chemical characterization of fine particle  
2 emissions from fireplace combustion of woods grown in the Midwestern and Western United  
3 States. *Environ. Eng. Sci.*, 21, 387-409, doi: 10.1089/109287504323067021, 2004b.

4 Fröhlich, R., Crenn, V., Setyan, A., Belis, C. A., Canonaco, F., Favez, O., Riffault, V.,  
5 Slowik, J. G., Aas, W., Aijälä, M., Alastuey, A., Artiñano, B., Bonnaire, N., Bozzetti, C.,  
6 Bressi, M., Carbone, C., Coz, E., Croteau, P. L., Cubison, M. J., Esser-Gietl, J. K.,  
7 Green, D. C., Gros, V., Heikkinen, L., Herrmann, H., Jayne, J. T., Lunder, C. R.,  
8 Minguillón, M. C., Močnik, G., O'Dowd, C. D., Ovadnevaite, J., Petralia, E., Poulain, L.,  
9 Priestman, M., Ripoll, A., Sarda-Estève, R., Wiedensohler, A., Baltensperger, U., Sciare, J.,  
10 and Prévôt, A. S. H.: ACTRIS ACSM intercomparison – Part 2: Intercomparison of ME-2  
11 organic source apportionment results from 15 individual, co-located aerosol mass  
12 spectrometers, *Atmos. Meas. Tech.*, 8, 2555-2576, doi:10.5194/amt-8-2555-2015, 2015.

13 Garbaras, A., Andriejauskiene, J., Bariseviciute, R. and Remeikis, V.: Tracing of atmospheric  
14 aerosol sources using stable carbon isotopes, *Lith. J. Phys.*, 48, 259-264,  
15 doi:10.3952/lithjphys.48309, 2008.

16 Garbaras, A., Masalaite, A., Garbariene, I., Ceburnis, D., Krugly, E., Remeikis, V., Puida, E.,  
17 Kvietkus, K., and Martuzevicius, D.: Stable carbon fractionation in size segregated aerosol  
18 particles produced by controlled biomass burning, *J. Aerosol Science*, 79, 86–96,  
19 doi:10.1016/j.jaerosci.2014.10.005, 2015.

20 Grieshop, A. P., Logue, J. M., Donahue, N. M., and Robinson, A. L.: Laboratory investigation  
21 of photochemical oxidation of organic aerosol from wood fires 1: measurement and  
22 simulation of organic aerosol evolution, *Atmos. Chem. Phys.*, 9, 1263–1277, doi:10.5194/acp-  
23 9-1263-2009, 2009.

24 Harrison, R. M., Beddows, D. C. S., Hu, L., Yin, J.: Comparison of methods for evaluation of  
25 wood smoke and estimation of UK ambient concentrations. *Atmos. Chem. Phys.*, 12, 8271 –  
26 8283, doi:10.5194/acp-12-8271-2012, 2012.

27 Hawkins, L. N., and Russell, L. M.: Oxidation of ketone groups in transported biomass  
28 burning aerosol from the 2008 Northern California Lightning Series fires, *Atmos. Environ.*,  
29 44, 4142-4154, doi:10.1016/j.atmosenv.2010.07.036, 2010.

1 Hennigan, C. J., Sullivan, A. P., Collett Jr., J. L., Robinson, A. L.: Levoglucosan stability in  
2 biomass burning particles exposed to hydroxyl radicals, *Geophys. Res. Lett.*, 37, L09806,  
3 doi:10.1029/2010GL043088, 2010.

4 Herich, H., Gianini, M. F. D., Piot, C., Mocnik, G., Jaffrezo, J. L., Besombes, J. L., Prévôt, A.  
5 S. H., and Hueglin, C.: Overview of the impact of wood burning emissions on carbonaceous  
6 aerosols and PM in large parts of the Alpine region, *Atmos. Environ.*, 89, 64–75,  
7 doi:10.1016/j.atmosenv.2014.02.008, 2014

8 Heringa, M. F., P. F. DeCarlo, R. Chirico, T. Tritscher, J. Dommen, E. Weingartner, R.  
9 Richter, G. Wehrle, A. S. H. Prevot, and Baltensperger U.: Investigations of primary and  
10 secondary particulate matter of different wood combustion appliances with a high-resolution  
11 time-of-flight aerosol mass spectrometer, *Atmos. Chem. Phys.*, 11(12), 5945-5957, 2011.

12 Hildebrandt, L., Kostenidou, E., Lanz, V. A., Prévôt, A. S. H., Baltensperger, U.,  
13 Mihalopoulos, N., Laaksonen, A., Donahue, N. M., and Pandis, S. N.: Sources and  
14 atmospheric processing of organic aerosol in the Mediterranean: insights from aerosol mass  
15 spectrometer factor analysis, *Atmos. Chem. Phys.*, 11, 12499–12515, doi:10.5194/acp-11-  
16 12499-2011, 2011.

17 Hoffmann, D., Tilgner, A., Iinuma, Y., and Hermann, H.: Atmospheric stability of  
18 levoglucosan: a detailed laboratory and modeling study, *Environ. Sci. Technol.*, 44, 694–699,  
19 doi:10.1021/es902476f, 2010.

20 Honrath, R., Owen, R. C., Val Martin, M., Reid, J., Lapina, K., Fialho, P., Dziobak, M.,  
21 Kleissl, J., and Westphal, D.: Regional and hemispheric impacts of anthropogenic and  
22 biomass burning emissions on summertime CO and O<sub>3</sub> in the North Atlantic lower free  
23 troposphere, *J. Geophys. Res.*, 109, doi:10.1029/2004JD005147, 2004.

24 Huang, R.-J., Zhang, Y., Bozzetti, C., Ho, K.-F., Cao, J.-J., Han, Y., Daellenbach, K. R.,  
25 Slowik, J. G., Platt, S. M., Canonaco, F., Zotter, P., Wolf, R., Pieber, S. M., Bruns, E. A.,  
26 Crippa, M., Ciarelli, G., Piazzalunga, A., Schwikowski, M., Abbaszade, G., Schnelle-Kreis,  
27 J., Zimmermann, R., An, Z., Szidat, S., Baltensperger, U., El Haddad, I., Prevot, A. S. H.:  
28 High secondary aerosol contribution to particulate pollution during haze events in China,  
29 *Nature*, 514(7521), 218-222, doi:10.1038/nature13774, 2014.

30 Jimenez, J. L., Canagaratna, M. R., Donahue, N. M., Prevot, A. S. H., Zhang, Q., Kroll, J. H.,  
31 DeCarlo, P. F., Allan, J. D., Coe, H., Ng, N. L., Aiken, A. C., Docherty, K. S., Ulbrich, I. M.,

1 Grieshop, A. P., Robinson, A. L., Duplissy, J., Smith, J. D., Wilson, K. R., Lanz, V. A.,  
2 Hueglin, C., Sun, Y. L., Tian, J., Laaksonen, A., Raatikainen, T., Rautiainen, J., Vaattovaara,  
3 P., Ehn, M., Kulmala, M., Tomlinson, J. M., Collins, D. R., Cubison, M. J., Dunlea, E. J.,  
4 Huffman, J. A., Onasch, T. B., Alfarra, M. R., Williams, P. I., Bower, K., Kondo, Y.,  
5 Schneider, J., Drewnick, F., Borrmann, S., Weimer, S., Demerjian, K., Salcedo, D., Cottrell,  
6 L., Griffin, R., Takami, A., Miyoshi, T., Hatakeyama, S., Shimono, A., Sun, J. Y., Zhang, Y.  
7 M., Dzepina, K., Kimmel, J. R., Sueper, D., Jayne, J. T., Herndon, S. C., Trimborn, A. M.,  
8 Williams, L. R., Wood, E. C., Middlebrook, A. M., Kolb, C. E., Baltensperger, U., and  
9 Worsnop, D. R.: Evolution of organic aerosols in the atmosphere, *Science*, 326, 1525 - 1529,  
10 doi:10.1126/science.1180353, 2009.

11 Kanamitsu, M., Ebisuzaki, W., Woollen, J., Yang, S. K., Hnilo, J. J., Fiorino, M., and Potter,  
12 G. L.: NCEP-DOE AMIP-II reanalysis (R-2), *Bull. Am. Meteorol. Soc.*, 83, 1631–1643,  
13 doi:10.1175/BAMS-83-11-1631, 2002.

14 Kikas, U., Reinart, A., Pugatshova, A., Tamm, E., and Ulevicius, V.: Microphysical, chemical  
15 and optical aerosol properties in the Baltic Sea region, *Atmos. Res.*, 90(2–4), 211–222,  
16 doi:10.1016/j.atmosres.2008.02.009, 2008.

17 Lanz, V. A., M. R. Alfarra, U. Baltensperger, B. Buchmann, C. Hueglin, and A. S. H. Prevot:  
18 Source apportionment of submicron organic aerosols at an urban site by linear unmixing of  
19 aerosol mass spectra, *Atmos. Chem. Phys.*, 7, 1503–1522, 2007.

20 Lanz, V. A., Prévôt, A. S. H., Alfarra, M. R., Weimer, S., Mohr, C., DeCarlo, P. F., Gianini,  
21 M. F. D., Hueglin, C., Schneider, J., Favez, O., D’Anna, B., George, C., and Baltensperger,  
22 U.: Characterization of aerosol chemical composition with aerosol mass spectrometry in  
23 Central Europe: an overview, *Atmos. Chem. Phys.*, 10, 10453–10471, doi:10.5194/acp-10-  
24 10453-2010, 2010.

25 Lavanchy, V. M. H., Gäggeler, H. W., Schotterer, U., Schwikowski, M., and Baltensperger,  
26 U.: Historical record of carbonaceous particle concentrations from a European high-alpine  
27 glacier (Colle Gnifetti, Switzerland), *J. Geophys. Res. Atmos.*, 104, 21227–21236,  
28 doi:10.1029/1999jd900408, 1999.

29 Lemire, K. R., Allen, D. T., Klouda, G. A., Lewis, C. W.: Fine particulate matter source  
30 attribution for southeast Texas using  $^{14}\text{C}/^{13}\text{C}$  ratios, *J. Geophys. Res.*, 107(D22), 4613,  
31 doi:10.1029/2002JD002339, 2002.



- 1 Levine, J. S. 1996. Biomass burning and global change, Cambridge, MA, MIT Press.
- 2 Lewis, C. W., Klouda, G. A., and Ellenson, W. D.: Radiocarbon measurement of the biogenic  
3 contribution to summertime PM-2.5 ambient aerosol in Nashville, TN, *Atmos. Environ.*, 38,  
4 6053–6061, doi:10.1016/j.atmosenv.2004.06.011, 2004.
- 5 Mann, G. W., Carslaw, K. S., Reddington, C. L., Pringle, K. J., Schulz, M., Asmi, A.,  
6 Spracklen, D. V., Ridley, D. A., Woodhouse, M. T., Lee, L. A., Zhang, K., Ghan, S. J., Easter,  
7 R. C., Liu, X., Stier, P., Lee, Y. H., Adams, P. J., Tost, H., Lelieveld, J., Bauer, S. E.,  
8 Tsigaridis, K., van Noije, T. P. C., Strunk, A., Vignati, E., Bellouin, N., Dalvi, M., Johnson,  
9 C. E., Bergman, T., Kokkola, H., von Salzen, K., Yu, F., Luo, G., Petzold, A., Heintzenberg,  
10 J., Clarke, A., Ogren, J. A., Gras, J., Baltensperger, U., Kaminski, U., Jennings, S. G.,  
11 O'Dowd, C. D., Harrison, R. M., Beddows, D. C. S., Kulmala, M., Viisanen, Y., Ulevicius, V.,  
12 Mihalopoulos, N., Zdimal, V., Fiebig, M., Hansson, H.-C., Swietlicki, E., and Henzing, J. S.:  
13 Intercomparison and evaluation of global aerosol microphysical properties among AeroCom  
14 models of a range of complexity, *Atmos. Chem. Phys.*, 14, 4679–4713, doi:10.5194/acp-14-  
15 4679-2014, 2014.
- 16 Masalaite, A., Remeikis, V., Garbaras, A., Dudoitis, V., Ulevicius, V., and Ceburnis, D.:  
17 Elucidating carbonaceous aerosol sources by the stable carbon  $\delta^{13}\text{C}_{\text{TC}}$  ratio in size-segregated  
18 particles, *Atmos. Res.*, 158–159, 1–12, doi:10.1016/j.atmosres.2015.01.014, 2015.
- 19 Matthew, B. M., Middlebrook, A. M., and Onasch, T. B.: Collection Efficiencies in an  
20 Aerodyne Aerosol Mass Spectrometer as a Function of Particle Phase for Laboratory  
21 Generated Aerosols, *Aerosol Sci. Tech.*, 42, 884–898, doi:10.1080/02786820802356797,  
22 2008.
- 23 Middlebrook, A. M., Bahreini, R., Jimenez, J. L., and Canagaratna, M. R.: Evaluation of  
24 composition-dependent collection efficiencies for the Aerodyne aerosol mass spectrometer  
25 using field data, *Aerosol Sci. Technol.*, 46, 258–271, doi:10.1080/02786826.2011.620041,  
26 2012.
- 27 Minguillón, M. C., Perron, N., Querol, X., Szidat, S., Fahrni, S. M., Alastuey, A., Jimenez, J.  
28 L., Mohr, C., Ortega, A. M., Day, D. A., Lanz, V. A., Wacker, L., Reche, C., Cusack, M.,  
29 Amato, F., Kiss, G., Hoffer, A., Decesari, S., Moretti, F., Hillamo, R., Teinilä, K., Seco, R.,  
30 Peñuelas, J., Metzger, A., Schallhart, S., Müller, M., Hansel, A., Burkhardt, J. F.,  
31 Baltensperger, U., and Prévôt, A. S. H.: Fossil versus contemporary sources of fine elemental

1 and organic carbonaceous particulate matter during the DAURE campaign in Northeast Spain,  
2 Atmos. Chem. Phys., 11, 12067-12084, doi:10.5194/acp-11-12067-2011, 2011.

3 Mochida, M., Kawamura, K., Fu, P. Q., and Takemura, T.: Seasonal variation of levoglucosan  
4 in aerosols over the western North Pacific and its assessment as a biomass-burning tracer,  
5 Atmos. Environ., 44, 3511–3518, doi:10.1016/j.atmosenv.2010.06.017, 2010.

6 MODIS NASA LANCE - FIRMS, 2011, MODIS Active Fire Detections, Data set, Available  
7 on – line: <http://earthdata.nasa.gov/data/nrt-data/firms>.

8 Mohr, C., Huffman, J. A., Cubison, M. J., Aiken, A. C., Docherty, K. S., Kimmel, J. R.,  
9 Ulbrich, I. M., Hannigan, M., and Jimenez, J. L.: Characterization of Primary Organic  
10 Aerosol 25 Emissions from Meat Cooking, Trash Burning, and Motor Vehicles with High-  
11 Resolution Aerosol Mass Spectrometry and Comparison with Ambient and Chamber  
12 Observations, Environ. Sci. Technol., 43, 2443–2449, doi:10.1021/es8011518, 2009.

13 Mordas, G., Ulevicius, V., Plauškaitė, K., Prokopčiuk, N.: Validation of the condensation  
14 particle counter UF-02M in laboratory and ambient conditions, Lith. J. Phys., 53 (3), 175-182,  
15 2013.

16 Ng, N. L., Herndon, S. C., Trimborn, A., Canagaratna, M. R. Croteau, P. L., Onasch, T. B.  
17 Sueper, D., Worsnop, D. R., Zhang, Q., Sun, Y. L. and Jayne, J. T.: An Aerosol Chemical  
18 Speciation Monitor (ACSM) for Routine Monitoring of the Composition and Mass  
19 Concentrations of Ambient Aerosol, Aerosol Sci. Tech., 45, 770-784,  
20 doi:10.1080/02786826.2011.560211, 2011.

21 Oanh, N. T. K., Ly, B. T., Tipayarom, D., Manandhar, B. R., Prapat, P., Simpson, C. D., Liu,  
22 L. J. S.: Characterization of particulate matter emission from open burning of rice straw.  
23 Atmos. Environ., 45, 493 - 502, doi:10.1016/j.atmosenv.2010.09.023 2011.

24 Orasche, J., Schnelle-Kreis, J., Abbaszade, G., and Zimmermann, R.: Technical Note: In-situ  
25 derivatization thermal desorption GC-TOFMS for direct analysis of particle-bound non-polar  
26 and polar organic species, Atmos. Chem. Phys., 11, 8977-8993, doi:10.5194/acp-11-8977-  
27 2011, 2011.

28 Orasche, J., Seidel, T., Hartmann, H., Schnelle-Kreis, J., Chow, J.C, Ruppert, H.,  
29 Zimmermann R.: Comparison of Emissions from Wood Combustion. Part 1: Emission

1 Factors and Characteristics from Different Small-Scale Residential Heating Appliances  
2 Considering Particulate Matter and Polycyclic Aromatic Hydrocarbon (PAH)-Related  
3 Toxicological Potential of Particle-Bound Organic Species, *Energy Fuels*, 26(11), 6695-6704,  
4 doi: 10.1021/ef301295k, 2012.

5 Oros, D. R., Radzi bin Abas, M., Omar, N. Y. M. J., Rahman, N. A., Simoneit, B. R. T.:  
6 Identification and emission factors of molecular tracers in organic aerosols from biomass  
7 burning: 3. Grasses. *Appl. Geochem.*, 21, 919–940, doi:10.1016/j.apgeochem.2006.01.008  
8 2006.

9 Paatero, P., and Tapper, U.: Positive matrix factorization – a nonnegative factor model with  
10 optimal utilization of error-estimates of data values, *Environmetrics*, 5, 111–126,  
11 doi:10.1002/env.3170050203, 1994.

12 Paatero, P.: Least squares formulation of robust non-negative factor analysis, *Chemometr.*  
13 *Intell. Lab.*, 37, 23–35, doi:10.1016/S0169-7439(96)00044-5, 1997.

14 Paatero, P., Eberly, S., Brown, S. G., and Norris, G. A.: Methods for estimating uncertainty in  
15 factor analytic solutions, *Atmos. Meas. Tech.*, 7, 781-797, doi:10.5194/amt-7-781-2014,  
16 2014.

17 Popovicheva, O., Kistler, M., Kireeva, E., Persiantseva, N., Timofeev, M., Kopeikin, V., and  
18 Kasper-Giebl, A.: Physicochemical characterization of smoke aerosol during large-scale  
19 wildfires: extreme event of August 2010 in Moscow, *Atmos. Environ.*, 96: 405–414,  
20 doi:10.1016/j.atmosenv.2014.03.026, 2014.

21 Puxbaum, H., Caseiro, A., Sánchez-Ochoa, A., Kasper-Giebl, A., Claeys, M., Gelencsér, A.,  
22 Legrand, M., Preunkert, S., and Pio, C.: Levoglucosan levels at background sites in Europe  
23 for assessing the impact of biomass combustion on the European aerosol background. *J.*  
24 *Geophys. Res.*, 112 (D23S05), doi:10.1029/2006JD008114, 2007.

25 Reid, J. S., Prins, E. M., Westphal, D. L., Schmidt, C. C., Richardson, K. A., Christopher, S.  
26 A., Eck, T. F., Reid, E. A., Curtis, C. A., Hoffman, J. P.: Real-time monitoring of South  
27 American smoke particle emissions and transport using a coupled remote sensing/box-model  
28 approach, *Geophys. Res. Lett.*, 31, L06107, doi:10.1029/2003GL018845, 2004.

29 Rutter, A. P., Snyder, D. C., Schauer, J. J., DeMinter, J. & Shelton, B. : Sensitivity and bias of

1 molecular marker-based aerosol source apportionment models to small contributions of coal  
2 combustion soot. *Environ. Sci. Technol.* 43, 7770-7777, 2009.

3 Saarikoski, S., Sillanpaa, M., Sofiev, M., Timonen, H., Saarnio, K., Teinela, K., Karppinen,  
4 A., Kukkonen, J., and Hillamo, R.: Chemical composition of aerosols during a major biomass  
5 burning episode over northern Europe in spring 2006: Experimental and modelling  
6 assessments, *Atmos. Environ.*, 41, 3577–3589, doi:10.1016/j.atmosenv.2006.12.053, 2007.

7 Salazar, G., Zhang, Y. L., Agrios, K., and Szidat, S.: Development of a method for fast and  
8 automatic radiocarbon measurement of aerosol samples by online coupling of an elemental  
9 analyzer with a MICADAS AMS, *Nucl. Instrum. Meth. Phys. Res. B.*, 361, 163-167,  
10 doi:10.1016/j.nimb.2015.03.051, 2015.

11 Sofiev, M., Siljamo, P., Valkama, I., Ilvonen, M., Kukkonen, J.: A dispersion modelling  
12 system SILAM and its evaluation against ETEX data, *Atm. Env.*, 40, 674–685,  
13 doi:10.1016/j.atmosenv.2005.09.069, 2006.

14 Sullivan, A. P., Holden, A. S., Patterson, L. A., McMeeking, G. R., Kreidenweis, S. M.,  
15 Malm, W. C., Hao, W. M., Wold, C. E. and Collett Jr. J. L.: A Method for Smoke Marker  
16 Measurements and its Potential Application for Determining the Contribution of Biomass  
17 Burning from Wildfires and Prescribed Fires to Ambient PM<sub>2.5</sub> Organic Carbon, *J. Geophys.*  
18 *Res.*, 113, D22302, doi:10.1029/2008JD010216, 2008.

19 Sullivan, A. P., A. A. May, T. Lee, G. R. McMeeking, S. M. Kreidenweis, S. K. Akagi, R. J.  
20 Yokelson, S. P. Urbanski and J. L. Collett, Jr.: Airborne characterization of smoke marker  
21 ratios from prescribed burning, *Atm. Chem. Phys.* 14(19): 10535-10545, 2014.

22 Sun, Y. L., Wang, Z. F., Dong, H. B., Yang, T., Li, J., Pan, X. L., Chen, P., Jayne, J. T.:  
23 Characterization of summer organic and inorganic aerosols in Beijing, China with an Aerosol  
24 Chemical Speciation Monitor, *Atmos. Environ.*, 51, 250–259,  
25 doi:10.1016/j.atmosenv.2012.01.013, 2012.

26 Szidat, S., Jenk, T. M., Gäggeler, H. W., Synal, H.-A., Fisseha, R., Baltensperger, U.,  
27 Kalberer, M., Samburova, V., Reimann, S., Kasper-Giebl, A., and Hajdas, I.: Radiocarbon  
28 (<sup>14</sup>C)-deduced biogenic and anthropogenic contributions to organic carbon (OC) of urban  
29 aerosols from Zurich, Switzerland, *Atmos. Environ.*, 38, 4035–4044,  
30 doi:10.1016/j.atmosenv.2004.03.066, 2004.

1 Szidat, S., Salazar, G. A., Vogel, E., Battaglia, M., Wacker, L., Synal, H.-A., and Türlér, A.:  
2  $^{14}\text{C}$  analysis and sample preparation at the new Bern Laboratory for the Analysis of  
3 Radiocarbon with AMS (LARA), *Radiocarbon*, 56, 561-566, doi:10.2458/56.17457, 2014.

4 Timonen, H., Aurela, M., Carbone, S., Saarnio, K., Saarikoski, S., Mäkelä, T., Kulmala, M.,  
5 Kerminen, V.-M. Worsnop, D. R. and Hillamo, R.. High Time-Resolution Chemical  
6 Characterization of the Water Soluble Fraction of Ambient Aerosols with PILS-TOC-IC and  
7 AMS. *Atmos. Meas. Tech.* 3:1063–1074, doi:10.5194/amt-3–1063-2010, 2010.

8 Turekian, V. C., Macko, S., Ballentine, D., Swap, R. J., and Garstang, M.: Causes of bulk  
9 carbon and nitrogen isotopic fractionations in the products of vegetation burns: laboratory  
10 studies, *Chem. Geol.*, 152, 181-192, doi:10.1016/S0009-2541(98)00105-3 1998.

11 Ulbrich, I. M., Canagaratna, M. R., Zhang, Q., Worsnop, D. R., and Jimenez, J. L.:  
12 Interpretation of organic components from Positive Matrix Factorization of aerosol mass  
13 spectrometric data, *Atmos. Chem. Phys.*, 9, 2891-2918, doi:10.5194/acp-9-2891-2009, 2009.

14 Ulevicius, V., Byčenkienė, S., Remeikis, V., Garbaras, A., Kecorius, S., Andriejauskienė, J.,  
15 Jasinevičienė, D., and Močnik, G.: Characterization of aerosol particle episodes in Lithuania  
16 caused by long-range and regional transport, *Atmos. Res.*, 98(2-4), 190-200,  
17 doi:10.1016/j.atmosres.2010.03.02, 2010a.

18 Ulevicius, V., Byčenkienė, S., Špirkauskaitė, N., and Kecorius, S.: Biomass burning impact  
19 on black carbon aerosol mass concentration at a coastal site: case studies, *Lith. J. Phys.*, 50(3),  
20 335–344, doi:10.3952/lithjphys.50304, 2010b.

21 Widory, D.: Nitrogen isotopes: Tracers of origin and processes affecting  $\text{PM}_{10}$  in the  
22 atmosphere of Paris, *Atmos. Environ.*, 41, 2382-2390, doi:10.1016/j.atmosenv.2006.11.009,  
23 2007.

24 Weimer, S., Alfarra, M.R., Schreiber, D., Mohr, M., Prevot, A.S.H., and Baltensperger U.:  
25 Organic aerosol mass spectral signatures from wood burning emissions: Influence of burning  
26 conditions and wood type, *J. Geophys. Res.*, 113, D10304, doi:10.1029/2007JD009309, 2008.

27 Wiedensohler, A., Birmili, W., Nowak, A., Sonntag, A., Weinhold, K., Merkel, M., Wehner,  
28 B., Tuch, T., Pfeifer, S., Fiebig, M., Fjåraa, A. M., Asmi, E., Sellegri, K., Depuy, R., Venzac,  
29 H., Villani, P., Laj, P., Aalto, P., Ogren, J. A., Swietlicki, E., Williams, P., Roldin, P.,  
30 Quincey, P., Hüglin, C., Fierz-Schmidhauser, R., Gysel, M., Weingartner, E., Riccobono, F.,  
31 Santos, S., Gruning, C., Faloon, K., Beddows, D., Harrison, R., Monahan, C., Jennings, S. G.,

1 O'Dowd, C. D., Marinoni, A., Horn, H.-G., Keck, L., Jiang, J., Scheckman, J., McMurry, P.  
2 H., Deng, Z., Zhao, C. S., Moerman, M., Henzing, B., de Leeuw, G., Löschau, G., and  
3 Bastian S.: Mobility particle size spectrometers: harmonization of technical standards and  
4 data structure to facilitate high quality long-term observations of atmospheric particle number  
5 size distributions. *Atmos. Meas. Tech.*, 5, 657–685. doi:10.5194/amt-5-657-2012, 2012.

6 Yttri, K. E., Simpson, D., Nøjgaard, J. K., Kristensen, K., Genberg, J., Stenström, K.,  
7 Swietlicki, E., Hillamo, R., Aurela, M., Bauer, H., Offenberg, J. H., Jaoui, M., Dye, C.,  
8 Eckhardt, S., Burkhardt, J. F., Stohl, A., and Glasius, M.: Source apportionment of the summer  
9 time carbonaceous aerosol at Nordic rural background sites, *Atmos., Chem. Phys.*, 11, 13339-  
10 13357, doi:10.5194/acp-11-13339-2011, 2011.

11 Yttri, K. E., Lund Myhre, C., Eckhardt, S., Fiebig, M., Dye, C., Hirdman, D., Ström, J.,  
12 Klimont, Z., and Stohl, A.: Quantifying black carbon from biomass burning by means of  
13 levoglucosan – a one-year time series at the Arctic observatory Zeppelin, *Atmos. Chem.*  
14 *Phys.*, 14, 6427-6442, doi:10.5194/acp-14-6427-2014, 2014.

15 Zawadzka, O., Makuch, P., Krzysztof, M., Markowicz, Zieliński, T., Petelski, T., Ulevicius,  
16 V., Strzałkowska, A., Rozwadowska, A., and Gutowska, D.: Studies of aerosol optical depth  
17 with the use of microtops II sun photometers and MODIS detectors in coastal areas of the  
18 Baltic Sea, *Acta Geophys.*, 62 (2), 400-422, doi:10.2478/s11600-013-0182-5, 2013.

19 Zhang, Y. L., Perron, N., Ciobanu, V. G., Zotter, P., Minguillon, M. C., Wacker, L., Prevot,  
20 A. S. H., Baltensperger, U., and Szidat, S.: On the isolation of OC and EC and the optimal  
21 strategy of radiocarbon based source apportionment of carbonaceous aerosols, *Atmos. Chem.*  
22 *Phys.*, 12 (22), 10841–10856, doi:10.5194/acp-12-10841-2012, 2012.

23 Zhang, Y.-L., Huang, R.-J., El Haddad, I., Ho, K.-F., Cao, J.-J., Han, Y., Zotter, P., Bozzetti,  
24 C., Daellenbach, K. R., Canonaco, F., Slowik, J. G., Salazar, G., Schwikowski, M., Schnelle-  
25 Kreis, J., Abbaszade, G., Zimmermann, R., Baltensperger, U., Prévôt, A. S. H., and Szidat, S.:  
26 Fossil vs. non-fossil sources of fine carbonaceous aerosols in four Chinese cities during the  
27 extreme winter haze episode of 2013, *Atmos. Chem. Phys.*, 15, 1299-1312, doi:10.5194/acp-  
28 15-1299-2015, 2015.

29 Zotter, P., Ciobanu, V. G., Zhang, Y. L., El-Haddad, I., Macchia, M., Daellenbach, K. R.,  
30 Salazar, G. A., Huang, R. J., Wacker, L., Hueglin, C., Piazzalunga, A., Fermo, P.,  
31 Schwikowski, M., Baltensperger, U., Szidat, S. and Prevot A. S. H.: Radiocarbon analysis of

1 elemental and organic carbon in Switzerland during winter-smog episodes from 2008 to 2012-  
2 Part 1: Source apportionment and spatial variability, *Atmos. Chem. Phys.*, 14(24), 13551-  
3 13570, 2014.

4

5



Figure 1. A) Map of the observation site, Preila (indicated by the red marker). Nearest major cities are Klaipeda (40 km north) and Kaliningrad (90 km south), B) Environmental pollution research station Preila and site surroundings (C).



1 Table 1. Preila site surroundings 10 km

Site altitude	5 (m) a.s.l.	Terrain below site	50.0 (%)
Median altitude	0 (m) a.s.l.	Standard deviation of altitude	7 (m)
Total population	6831	Standard deviation of population	159
Mean population density	20 (km <sup>-2</sup> )	Standard deviation of population density	13 (km <sup>-2</sup> )
Local population density	29.5 (km <sup>-2</sup> )		
Dominating land cover types (based on GLC2000)			
Water bodies (natural & artificial) (20)			84.9 (%)
Tree cover, needle-leaved, evergreen (4)			13.2 (%)
Tree cover, mixed leaf type (6)			1.1 (%)
Herbaceous cover, closed-open (13)			0.4 (%)

2

3

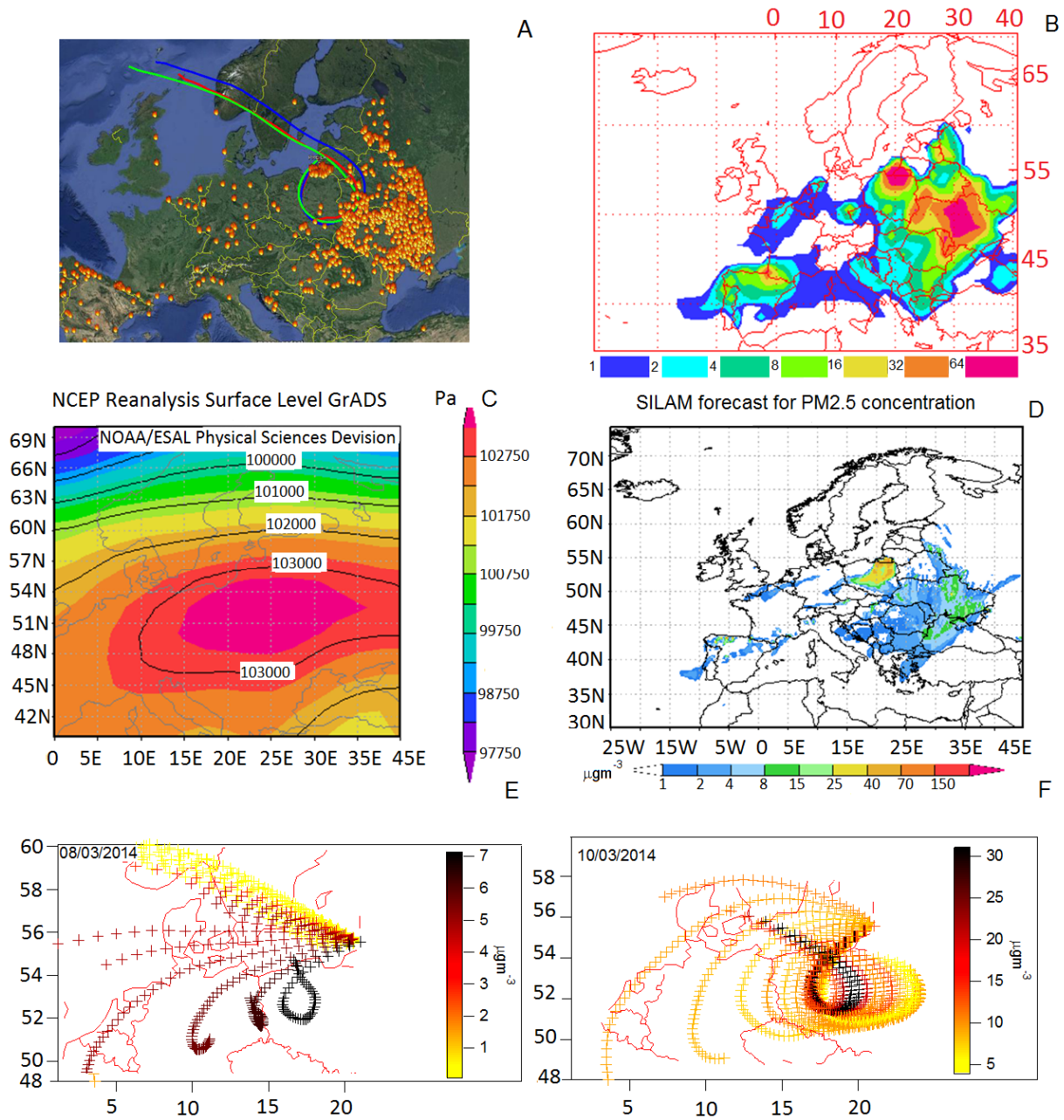


Figure 2. (A) Combined MODIS images observed from the Aqua satellite on 10 March 2014, showing numerous fires due to seasonal grass burning and 72-hour air mass backward trajectories from the fire regions arriving at Preila at 100 (red), 200 (blue) and 500 (green) m above ground level (AGL). (B) NAAPS model results showing surface smoke concentrations for the strongest stage (10 March 2014) (the color scale (from blue to purple) corresponds to the 7 levels of the contours that indicate the smoke mass mixing ratio ( $\mu\text{g m}^{-3}$ ) at the surface. Smoke optical depth at a wavelength of 0.55 microns. The contouring begins at 1  $\mu\text{g m}^{-3}$  and

1 doubles in magnitude for each successive contour. (C) Pressure level at surface at 2.5 degree  
2 latitude  $\times$  2.5 degree longitude global grids in Pa (NCEP/NCAR Reanalysis 1, 10 March  
3 2014). (D) PM<sub>2.5</sub> concentration ( $\mu\text{g m}^{-3}$ ) forecast utilized by the SILAM chemical transport  
4 model during the event of grass fires, E,F) ACSM organic concentration ACSM organics  
5 concentration ( $\mu\text{g m}^{-3}$ ) (measured in Preila) weighted air mass back trajectories of 48 h (an  
6 arrival on 8 (left) and 10 (right) March 2014) with an altitude endpoint of 500 m AGL.

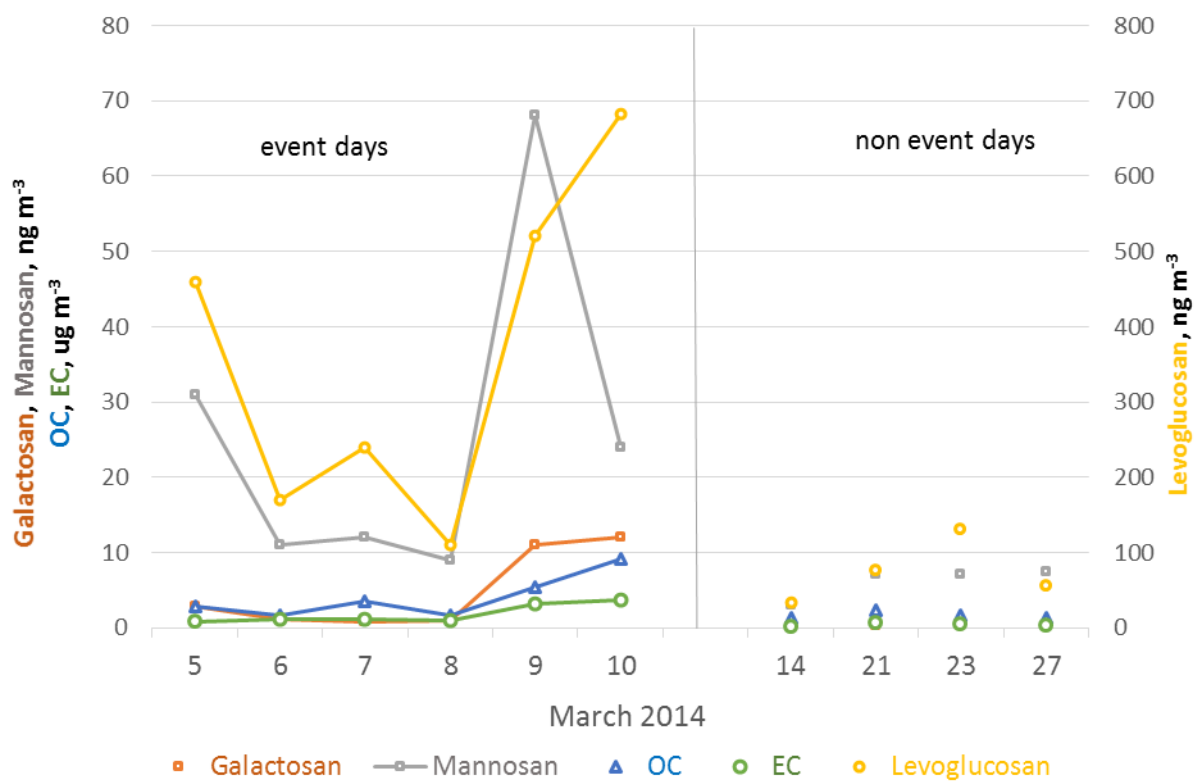
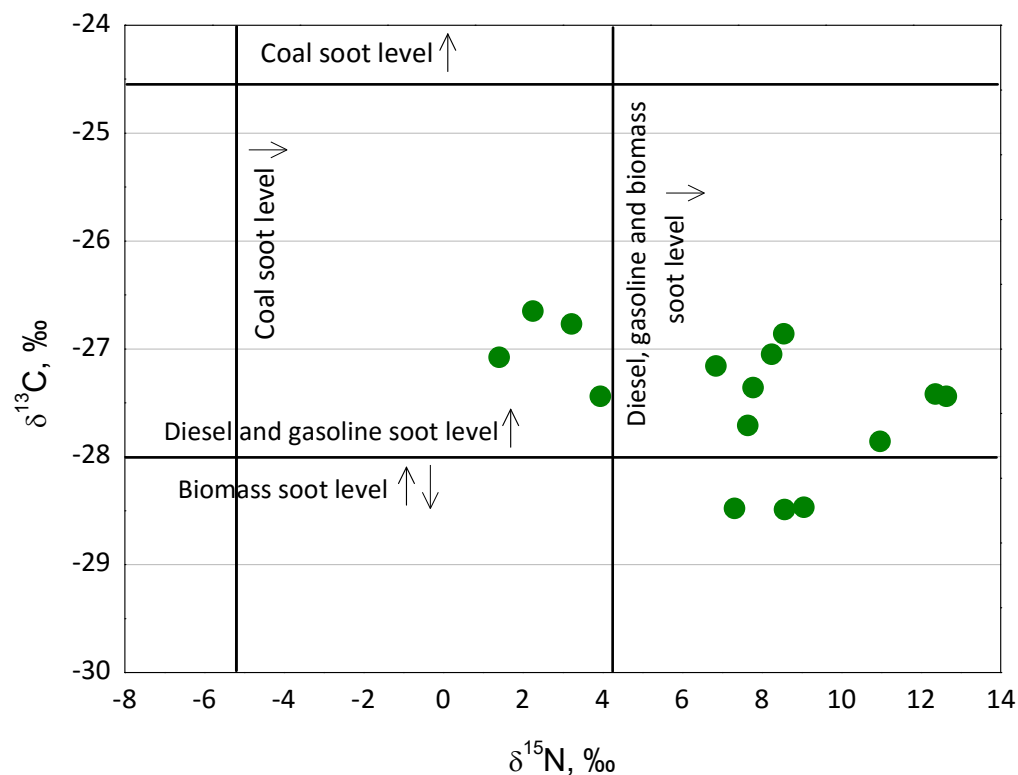


Figure 3. Average daily concentration during event days (from 5 to 10 March 2014) and non-event days (14<sup>th</sup>, 21<sup>th</sup>, 23<sup>th</sup> and 27<sup>th</sup> March 2014) for levoglucosan, galactosan, mannosan (in ng m<sup>-3</sup>) and for elemental carbon (EC) and organic carbon (OC) in µg m<sup>-3</sup>.

1



2

3 Figure 4. Stable carbon and nitrogen isotope ratio values of  $\text{PM}_{10}$  in Preila station. Vertical and  
 4 horizontal lines represent carbon and nitrogen, respectively, isotope ratio characteristic values  
 5 for the sources of aerosol particles (Garbaras et al., 2008, 2015; Ulevicius et al., 2010a;  
 6 Widory 2007).

7

1 Table 2. Variation of the fractions of EC<sub>f</sub>, EC<sub>nf</sub>, OC<sub>f</sub>, OC<sub>nf</sub> and TC, EC and OC values during  
2 the study periods.

$\mu\text{g m}^{-3}/\text{date of collection}$	EC <sub>f</sub>	EC <sub>nf</sub>	OC <sub>f</sub>	OC <sub>nf</sub>	TC	EC	OC
2014.03.05	0.25±0.04	0.33	0.47±0.10	2.34±0.18	3.39±0.18	0.59±0.17	2.80±0.18
2014.03.07	0.21±0.04	0.61	0.39±0.12	2.80±0.20	4.01±0.23	0.81±0.24	3.31±0.20
2014.03.08	0.15±0.05	0.26	0.56±0.07	1.46±0.12	2.43±0.13	0.41±0.18	2.24±0.15
2014.03.09	0.46±0.16	0.95	0.95±0.18	4.98±0.36	7.28±0.43	1.36±0.63	6.32±0.35
2014.03.10	0.56±0.18	1.64	1.64±0.28	7.77±0.50	11.72±0.64	2.31±0.75	9.47±0.51

3

4

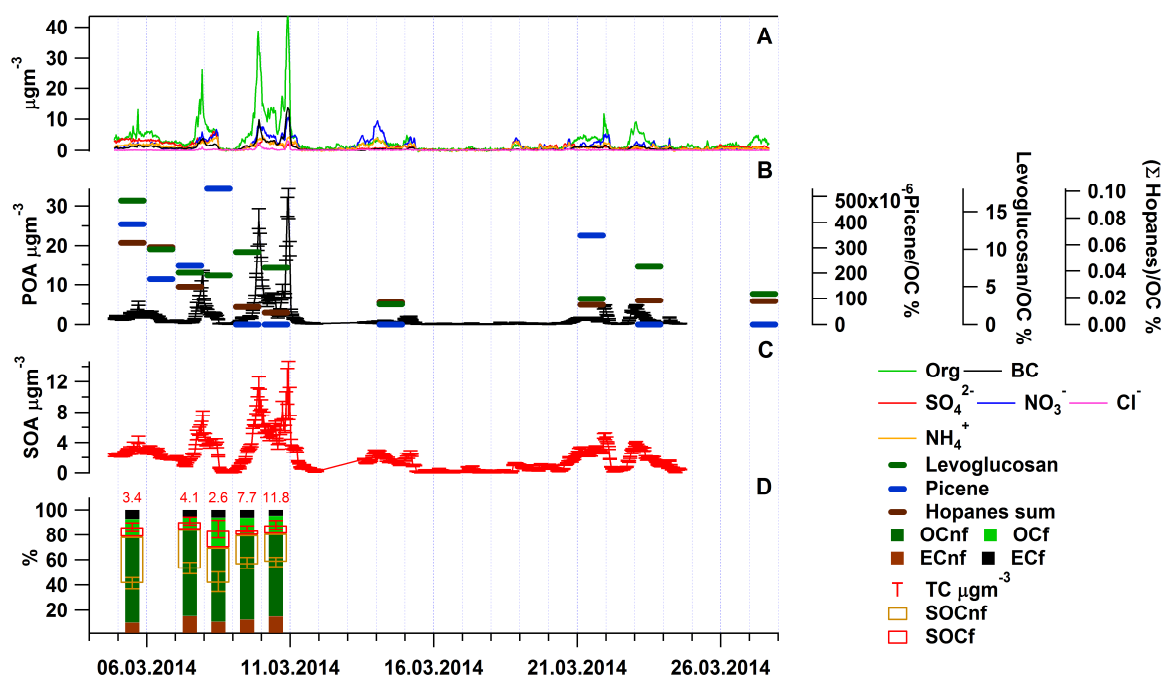


Figure 5. Average chemical composition and time series of NR-PM<sub>1</sub> OA for the entire study (A), B) Time series of the POA factor and percent contribution of the corresponding tracer species (levoglucosan, picene and hopanes) to total OA, C) Time series of the SOA factor, D) Relative source apportionment of TC during BB event. Numbers indicate the total carbon absolute concentrations in µg m<sup>-3</sup>, variations of the mass concentrations of the SOC<sub>f</sub> and SOC<sub>nf</sub> (the whiskers above and below the boxes indicate the 1<sup>st</sup> and 3<sup>rd</sup> quartiles).

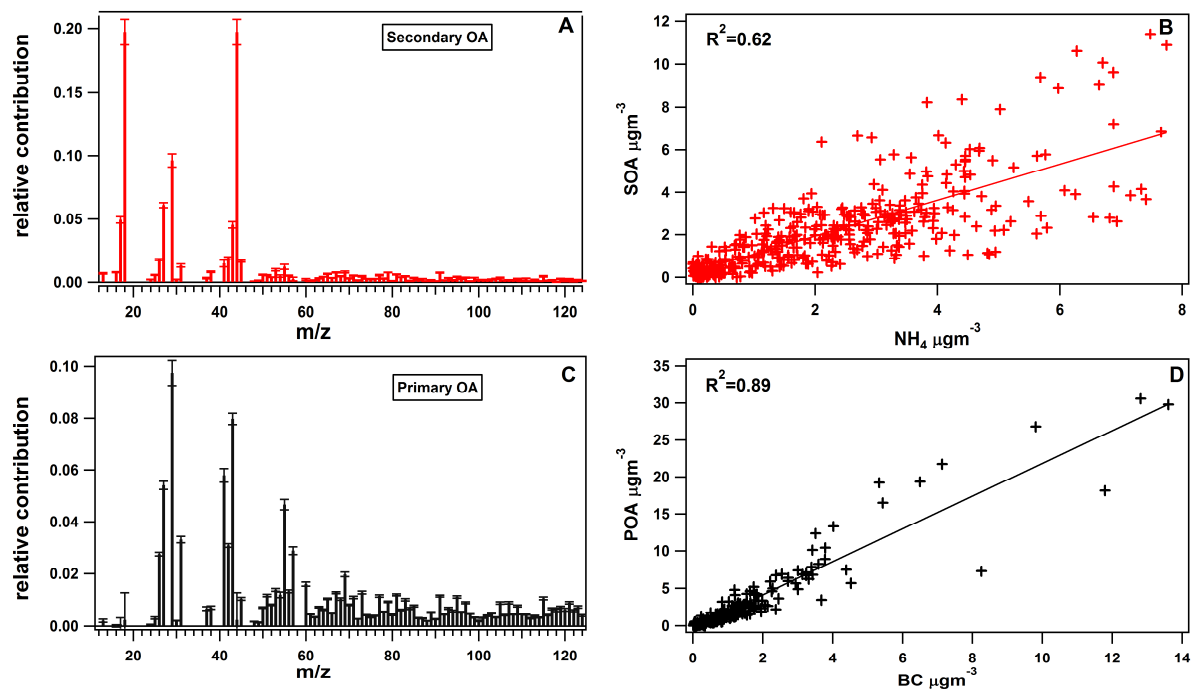


Figure 6. Mass spectra of SOA and POA, error bars represent the standard deviation of 20 PMF runs (A,C) and the scatter plots illustrate the relationship between SOA and  $\text{NH}_4^+$  (B) and POA with BC (D).



1 Table 3. Average Percentage Contributions of Different Sources

Relative contributions [%] to TC	POC <sub>f</sub>	POC <sub>nf</sub>	SOC <sub>f</sub>	SOC <sub>nf</sub>	EC <sub>f</sub>	EC <sub>nf</sub>	TC to PM1
2014.03.05	5.07	43.23	6.69	22.51	9.66	12.83	28.44
2014.03.07	6.26	43.58	5.66	19.14	6.58	18.79	37.62
2014.03.08	7.73	26.28	13.36	18.65	12.60	21.38	24.80
2014.03.09	4.55	41.30	4.38	13.12	12.48	24.17	51.27
2014.03.10	6.82	43.02	5.9	14.83	7.18	22.26	43.91
Relative contributions [%] to OC	POC <sub>f</sub>	POC <sub>nf</sub>	SOC <sub>f</sub>	SOC <sub>nf</sub>			
2014.03.05	6.55	55.78	8.63	29.04			
2014.03.07	8.39	58.38	7.59	25.64			
2014.03.08	11.70	39.80	20.24	28.25			
2014.03.09	7.18	65.20	6.91	20.71			
2014.03.10	9.66	60.96	8.36	21.02			

2

3

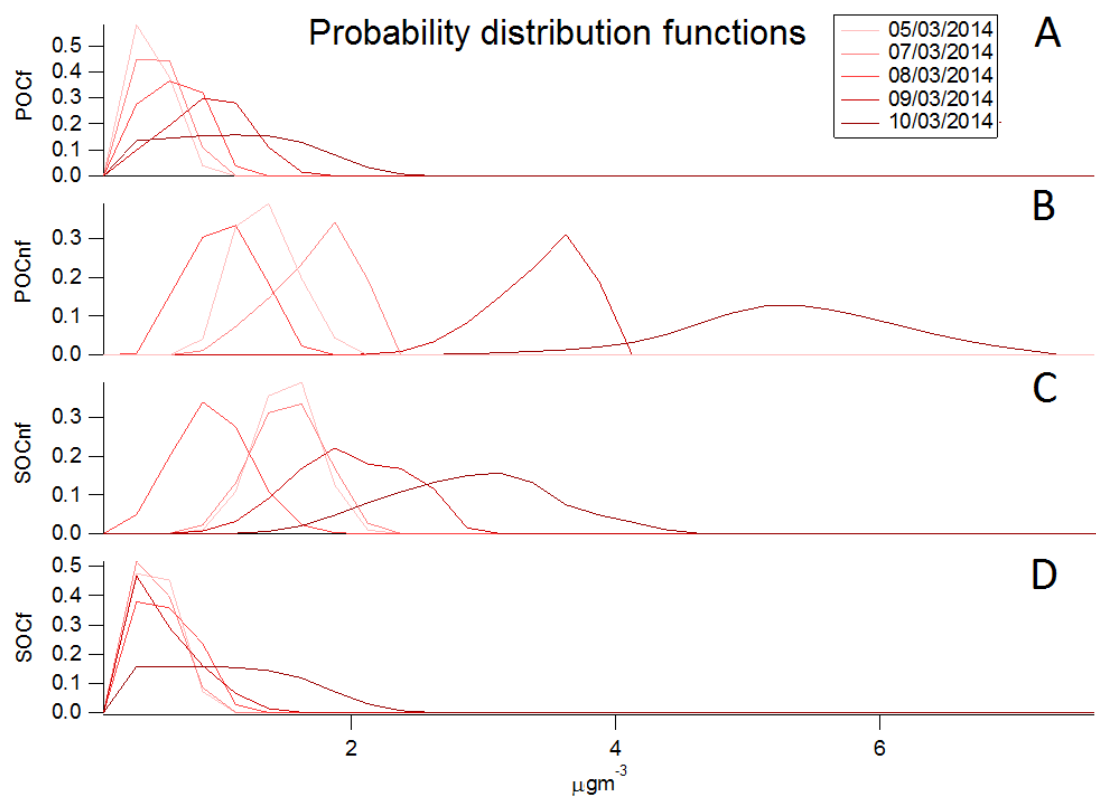


Figure 7. Probability distribution functions of the absolute daily contribution of  $\text{POC}_f$  (A),  $\text{POC}_{nf}$  (B),  $\text{SOC}_{nf}$  (C),  $\text{SOC}_f$  (D).

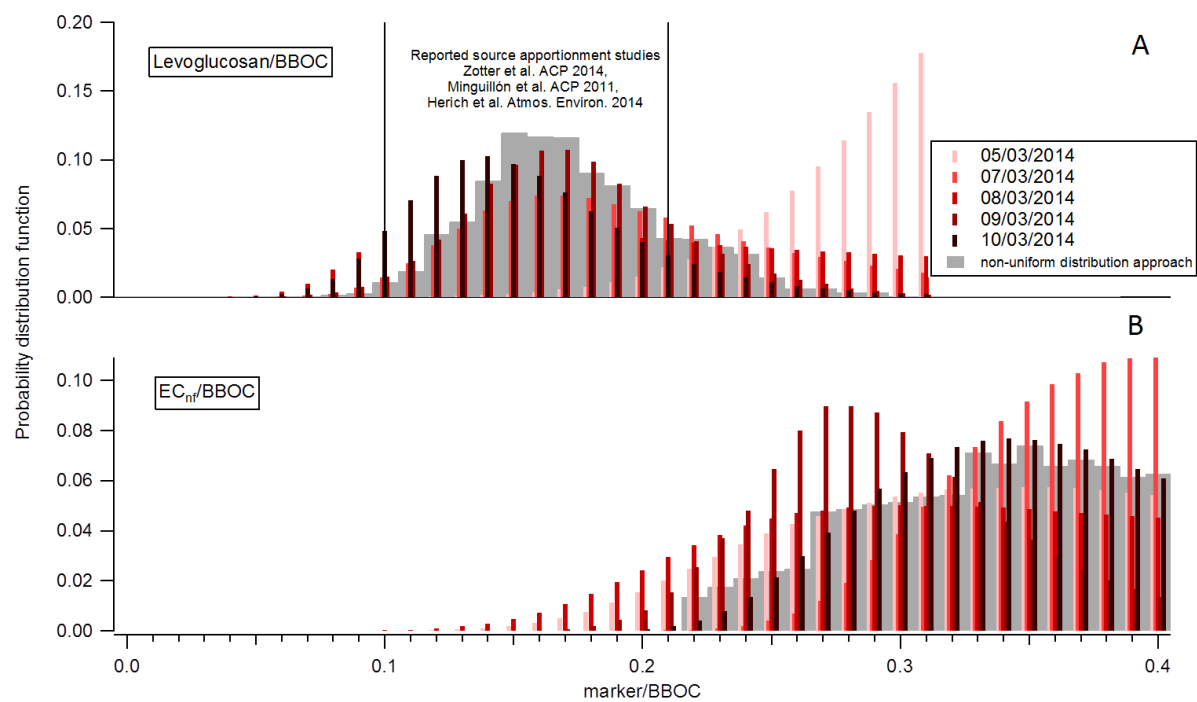


Figure 8. Probability distribution functions of Levoglucosan/BBOC (A) and EC<sub>nf</sub>/BBOC (B).